

# EQUAL- AND UNEQUAL-MASS MERGERS OF DISK AND ELLIPTICAL GALAXIES WITH BLACK HOLES: THE $M_{\text{BH}} - \sigma$ AND $M_{\text{BH}} - M_*$ RELATIONS

PETER H. JOHANSSON<sup>1</sup>, THORSTEN NAAB<sup>1</sup>, ANDREAS BURKERT<sup>1</sup>

<sup>1</sup> Universitäts-Sternwarte München, Scheinerstr. 1, D-81679 München, Germany; pjoan@usm.lmu.de

Submitted to ApJ.

## ABSTRACT

We present binary galaxy merger simulations with varying mass ratios and different progenitor morphologies. The simulations include mergers of gas-rich disks (Sp-Sp), of early-type galaxies and disks (E-Sp, mixed mergers), and mergers of early-type galaxies (E-E, dry mergers). We follow the dynamics of gas, stars and dark matter, and include radiative cooling, star formation and black hole (BH) accretion and the associated feedback processes as in Springel et al. We study the mass assembly of the BHs and discuss technical issues of the implemented model in detail. For Sp-Sp mergers, the peak star formation rate and BH accretion rate decrease and the growth timescales of the central black holes and newly formed stars increase with higher progenitor mass ratios. The peak BH accretion rate typically occurs shortly after the time of BH merging for low progenitor mass ratios (e.g. 3:1 and lower), whereas for higher progenitor mass ratios there is no clear correlation between the peak BH accretion rate and BH merging time. The termination of star formation by BH feedback in disk mergers is significantly less important for higher progenitor mass ratios (e.g. 3:1 and higher). In addition, the inclusion of BH feedback suppresses efficiently star formation in dry E-E mergers and mixed E-Sp mergers. All merger remnants, independent of their progenitors, follow the observed relations between the central BH mass and the stellar velocity dispersion ( $M_{\text{BH}} - \sigma$ ) and the bulge mass ( $M_{\text{BH}} - M_*$ ), with the dominant source of scatter arising from variations in the initial gas mass fraction. The normalizations for both relations and the simulated slope of the ( $M_{\text{BH}} - \sigma$ ) relation are in good agreement with the observations, whereas the simulated slope of the ( $M_{\text{BH}} - M_*$ ) relation is slightly steeper compared to the observations. This indicates that the simple BH feedback model self-regulates the mass growth of the BHs in accordance with the observed relations for a very wide range of merger progenitors.

*Subject headings:* galaxies: interaction – galaxies: active galaxies: evolution – galaxies: formation – methods: numerical

## 1. INTRODUCTION

Observations in the last decade have shown that supermassive black holes (BH) reside in the centers of most if not all galaxies with spheroids (e.g. Kormendy & Richstone 1995; Richstone et al. 1998). The properties of these black holes and their host galaxies are correlated in a number of ways, e.g. the correlation of the BH mass and the bulge velocity dispersion as expressed in the  $M_{\text{BH}} - \sigma$  relation (e.g. Ferrarese & Merritt 2000; Gebhardt et al. 2000; Tremaine et al. 2002) and the relation between BH mass and the bulge stellar mass,  $M_{\text{BH}} - M_{\text{bulge}}$  (e.g. Magorrian et al. 1998; Marconi & Hunt 2003; Häring & Rix 2004). These observed relations indicate that supermassive BHs and the stellar spheroids of their host galaxies do not form independently of each other.

There exists several theoretical explanations for the observed correlation between galaxy properties and the black hole mass, including physical mechanisms such as viscous disk accretion and star formation (Burkert & Silk 2001), gas or dark matter collapse (Adams et al. 2001), dissipationless merging (Ciotti & van Albada 2001) and the merging and migration of massive stellar clumps and their associated intermediate-mass BHs to the galactic centers (Bournaud et al. 2007a; Elmegreen et al. in prep). The majority of the models rely on some form of self-regulated BH mass growth, in which gas

is fed to the central black hole until the black hole releases sufficient energy to unbind the gas and blow it away in momentum- or pressure-driven winds (e.g. Ciotti & Ostriker 1997; Silk & Rees 1998; Fabian 1999; Murray et al. 2005; Ciotti & Ostriker 2007).

The first theoretical studies of the co-evolution of black holes and galaxies were carried out using semi-analytic modeling (SAM) techniques (e.g. Cattaneo et al. 1999; Kauffmann & Haehnelt 2000; Wyithe & Loeb 2003; Volonteri et al. 2003; Granato et al. 2004; Croton et al. 2006; Bower et al. 2006). In SAMs the evolution of the dark matter halos is followed with merger trees and the evolution of the galaxies and their embedded black holes is modeled with simple physical parameterizations. Most SAMs are based on the assumption that quasar activity is triggered by major galaxy mergers of gas-rich galaxies, in which large quantities of gas flow to the centers of galaxies (e.g. Barnes & Hernquist 1996; Kazantzidis et al. 2005; Naab et al. 2006a; Hopkins et al. 2007b) producing starbursts and leading to rapid black hole growth (Hernquist 1989). During the mergers the dominant dynamical process is the violent relaxation (Lynden-Bell 1967; Arad & Johansson 2005) of the stellar and dark matter components.

This picture is supported by observations of local mergers that show large central gas concentrations, accompanied by strong starburst and AGN activity (Genzel et al.

1998), indicating BH growth. These so called ultraluminous infrared galaxies (ULIRGs) mostly originate from major mergers, typically with mass ratios below 3:1 (e.g. Dasyra et al. 2006a,c; Väisänen et al. 2007). The ULIRGs could eventually evolve into spheroidal galaxies (Hibbard & Yun 1999; Genzel et al. 2001; Rothberg & Joseph 2006; Dasyra et al. 2006b). In addition, nearby quasars (e.g. McLure et al. 1999; Canalizo & Stockton 2001) are preferentially found in tidally disturbed objects, thus corroborating the important role of galaxy interactions and mergers for major black hole growth. Furthermore, an increasing number of recent infrared and X-ray surveys have completed the census of BH activity and mass growth by revealing a significant population of highly obscured AGNs at redshifts above  $z \sim 1$  (Johansson et al. 2004; Houck et al. 2005; Barger et al. 2005).

A first, simple self-consistent method for including black hole growth and thermal feedback coupling to the surrounding gas in simulations of binary disk galaxy mergers was developed by Springel et al. (2005b). Based on this description hydrodynamical simulations of BH growth in galaxy mergers were used to reproduce the local  $M_{\text{BH}} - \sigma$  relation (Di Matteo et al. 2005), study the redshift evolution of this relation (Robertson et al. 2006b), provide an explanation of the red colors of massive ellipticals (Springel et al. 2005a), and describe the fundamental plane of elliptical galaxies (Robertson et al. 2006a). Using this black hole merger sample Hopkins et al. (2005, 2006) proposed a comprehensive picture of a unified merger-driven model for the origin of starbursts, quasars and their relation to galaxy spheroid formation. Recently, simulations of both individual galaxies (Khalatyan et al. 2007) and larger cosmological volumes (Sijacki et al. 2007; Di Matteo et al. 2007) with BH feedback starting directly from initial conditions appropriate for the  $\Lambda$ CDM cosmology have been performed. Both cosmological studies assumed that seed black holes were present at high redshifts in forming halos and then followed their evolution self-consistently with hydrodynamical simulations. Di Matteo et al. (2007) employed the Springel et al. (2005b) black hole feedback prescription, whereas Sijacki et al. (2007) used in addition a predominantly mechanical feedback model for black holes in galaxy clusters with low accretion rates, in which AGN-driven bubbles are injected into a gaseous environment (Sijacki & Springel 2006). The study by Di Matteo et al. (2005) showed that the  $M_{\text{BH}} - \sigma$  relation can be reproduced for equal-mass disk galaxy mergers. The cosmological studies of Sijacki et al. (2007) and Di Matteo et al. (2007) naturally include mergers with a range in mass ratios and morphologies, and both studies are able to find adequate fits to the observed  $M_{\text{BH}} - \sigma$  and  $M_{\text{BH}} - M_*$  relations at both high and low redshifts, where  $M_*$  is defined as the total stellar mass within the effective radius. However, even the highest resolution cosmological simulations resolve spatial scales that are an order of magnitude larger than the typical spatial scales resolvable in high-resolution merger simulations ( $\epsilon \sim 0.1h^{-1}\text{kpc}$ ) and it is not obvious that low-resolution simulations that only resolve scales corresponding to the effective radii for typical galaxies are able to capture the essential physics related to BH feedback.

In a cosmological context unequal-mass mergers are

more frequent than equal-mass mergers and the progenitors will have varying morphologies (Khochfar & Burkert 2001; Khochfar & Silk 2006b). It has been shown that the mass ratio of disk mergers has a significant impact on the remnant properties. Equal-mass disk mergers predominantly result in slowly rotating systems with boxy or disky isophotes, whereas unequal-mass mergers lead to rotating, intrinsically anisotropic spheroids with disky isophotes (Barnes 1998; Naab et al. 1999; Cretton et al. 2001; Barnes 2002; Naab & Burkert 2003; Bournaud et al. 2005; Burkert & Naab 2005; Cox et al. 2006; Burkert et al. 2007). The mass ratio and the actual gas content have a significant influence on the final stellar orbit structure and internal kinematics of the merger remnants (Barnes & Hernquist 1996; Jesseit et al. 2005, 2007; Thomas et al. 2007). Apparently, binary mergers of disk galaxies with varying mass ratios are one reasonable mechanism for the formation of intermediate- and low-mass ellipticals, whereas more massive slowly rotating ellipticals are probably formed in multiple mergers at high redshifts (Naab et al. 2007; Burkert et al. 2007). A potential assembly mechanism for massive boxy and slowly-rotating elliptical galaxies at low redshift is merging of gas-poor early-type galaxies (dry mergers) (Naab et al. 2006b). There is now mounting observational evidence for dry galaxy mergers both in galaxy clusters (van Dokkum et al. 1999; Tran et al. 2005) and in the field (van Dokkum 2005; Bell et al. 2006). Simulations of gas-free mergers have been shown to preserve the fundamental plane of elliptical galaxies (Nipoti et al. 2003; Boylan-Kolchin et al. 2005). Furthermore Robertson et al. (2006a) showed that E-E mergers including BH feedback physics do not strongly alter the original  $M_{\text{BH}} - \sigma$  relation, although they might be the source for some of the observed scatter in the relation. Mixed merging, in which a gas-poor early-type galaxy merges with a gas-rich spiral disk galaxy might also form elliptical galaxies with distinct properties. They were shown by Khochfar & Burkert (2003, 2005); Naab et al. (2006b); Hopkins et al. (2007a) to dominate the merger budget at intermediate masses between the low-mass ellipticals Sp-Sp mergers and the highest mass E-E mergers. Thus it is of utmost importance to study whether the current BH feedback model that reproduces the  $M_{\text{BH}} - \sigma$  and  $M_{\text{BH}} - M_*$  relations for equal-mass disk mergers, is also able to reproduce the observed relations in galaxy mergers with varying mass ratios and progenitor morphologies.

In this paper we present simulations of unequal-mass disk mergers, mixed E-Sp mergers and E-E mergers, including BH feedback. Our aim is to study the observed local  $M_{\text{BH}} - \sigma$  and  $M_{\text{BH}} - M_*$  relations and see whether they hold for our merger sample with varying mass ratios and different progenitor morphologies. We also study in detail the effect of varying the merger mass ratio on the peak BH accretion rate and final BH mass. In addition, we analyse the termination of star formation by BH feedback in unequal-mass disk mergers, mixed E-Sp mergers and dry E-E mergers compared to equal-mass disk mergers (Springel et al. 2005a). Furthermore, we discuss in detail the modeling of black hole mergers in the Springel et al. (2005b) feedback prescription. The merging of black holes is not resolved in the numerical simulations and therefore an effective model for BH merging

needs to be adopted. We show that the assumption of rapid merging of the black holes in equal- and unequal-mass galaxy mergers is critical for reproducing the final BH mass that fulfills the observed relations using the self-regulated Springel et al. (2005b) BH feedback model.

This paper is structured as follows. In §2 we describe the simulation code and discuss the BH feedback and merger prescriptions. The galaxy model and merger setups, together with the adopted parameter settings, are discussed in §3. Here we also simulate a set of isolated disk galaxies and perform a detailed analysis of the effect of the merger prescription and resolution on the growth and final mass of the BHs. In §4 we present the results and implications of our Sp-Sp, mixed E-Sp and dry E-E simulation sets to the origin of the  $M_{\text{BH}} - \sigma$  and  $M_{\text{BH}} - M_*$  relations. In addition we perform here a detailed study of BH and star formation activity as a function of merger mass ratio. Finally, we summarize and discuss our findings in §5.

## 2. METHODOLOGY

### 2.1. Numerical code

We perform the simulations using the parallel TreeSPH-code GADGET-2 (Springel 2005). The code follows the gas dynamics using the Lagrangian Smoothed Particle Hydrodynamics (SPH) (e.g. Monaghan 1992) technique formulated in such a way that energy and entropy is manifestly conserved (Springel & Hernquist 2002). Following Katz et al. (1996) the radiative cooling for a primordial mixture of hydrogen and helium together with a spatially uniform time-independent local UV background (Haardt & Madau 1996) is included.

We include star formation and the associated supernova feedback, but exclude supernova-driven galactic winds, following the sub-resolution multiphase model developed by Springel & Hernquist (2003). In this model the ISM is treated as a two-phase medium in which cold clouds are embedded in a tenuous hot gas at pressure equilibrium. Stars form from the cold clouds in regions where  $\rho > \rho_{\text{th}}$  with the shortlived stars supplying an energy of  $10^{51}$  ergs to the surrounding gas by supernovae. The threshold density,  $\rho_{\text{th}}$ , is determined self-consistently in the model by requiring that the equation-of-state (EOS) is continuous at the onset of star formation. The black hole feedback is modeled in a similar fashion with an effective model following Springel et al. (2005b). In what follows we will briefly summarize the most relevant aspects of the Springel et al. (2005b) black hole feedback model and the associated description for BH mergers.

### 2.2. Black hole feedback

The growth of the supermassive black holes is followed with an effective subresolution model in which the unresolved accretion onto the BH is related to the resolved gas distribution using a Bondi-Hoyle-Lyttleton parameterization (Hoyle & Lyttleton 1939; Bondi & Hoyle 1944; Bondi 1952). In this description, the accretion rate onto the BH is given by

$$\dot{M}_{\text{B}} = \frac{4\pi\alpha G^2 M_{\text{BH}}^2 \rho}{(c_s^2 + v^2)^{3/2}}. \quad (1)$$

Here  $\rho$  and  $c_s$  are the density and sound speed of the surrounding gas, respectively,  $v$  is the velocity of the BH

relative to the surrounding gas and  $\alpha$  is a dimensionless parameter setting the efficiency of the accretion. In addition, it is assumed that the maximum accretion is limited to the Eddington rate

$$\dot{M}_{\text{edd}} = \frac{4\pi G M_{\text{BH}} m_{\text{p}}}{\epsilon_{\text{r}} \sigma_{\text{T}} c}, \quad (2)$$

where  $m_{\text{p}}$  is the proton mass,  $\epsilon_{\text{r}}$  is the radiative efficiency and  $\sigma_{\text{T}}$  is the Thomson cross-section. Thus the accretion rate is given by

$$\dot{M}_{\text{BH}} = \min(\dot{M}_{\text{B}}, \dot{M}_{\text{edd}}). \quad (3)$$

The radiative efficiency,  $\epsilon_{\text{r}}$  simply gives the mass to energy conversion efficiency

$$\epsilon_{\text{r}} = \frac{L_{\text{r}}}{\dot{M}_{\text{BH}} c^2}, \quad (4)$$

for which we adopt the fixed value of  $\epsilon_{\text{r}} = 0.1$  following Springel et al. (2005b), who base this value on the mean value for radiatively efficient Shakura & Syun'yaev (1973) accretion onto a Schwarzschild BH. Finally some fraction  $\epsilon_{\text{f}}$  of the radiated luminosity  $L_{\text{r}}$  couples thermally and isotropically to the surrounding gas in the form of black hole feedback energy resulting in

$$\dot{E}_{\text{feed}} = \epsilon_{\text{f}} L_{\text{r}} = \epsilon_{\text{f}} \epsilon_{\text{r}} \dot{M}_{\text{BH}} c^2. \quad (5)$$

Again, following Springel et al. (2005b), we fix  $\epsilon_{\text{f}} = 0.05$  so that in total 0.5 per cent of the accreted rest mass energy is available as feedback. This choice fixes the normalization of the  $M_{\text{BH}} - \sigma$  relation and reproduces the observed relation in equal-mass binary galaxy merger simulations with BH feedback as was shown by Di Matteo et al. (2005). The feedback energy is distributed as thermal energy to the surrounding gas particles weighted with the SPH kernel.

Numerically the BHs are represented as collisionless 'sink' particles, which only feel gravitational forces. The properties, such as density, temperature and the bulk velocity of the local gas around the BH are estimated in a similar fashion to normal SPH particles. Based on these quantities and the equations above, the BH accretion rate is then estimated.

The actual accretion of gas particles is performed, using a stochastic approach, in a similar fashion to spawning star particles from gas in the star formation prescription. For details, see Springel & Hernquist (2003); Springel et al. (2005b). In low-resolution simulations this method can become quite noisy, when a single accreted gas particle can substantially change the mass of the BH particle. To circumvent this problem Springel et al. (2005b) introduced an internal degree of freedom for the BH particle that describes the BH mass in a smooth fashion in the case of ideal resolution. The internal BH mass is then used to compute the accretion rates. The mass growth of the BH is followed both in terms of the internal mass and the dynamical mass, with the dynamical mass only growing in discrete steps as opposed to the smoothly growing internal mass.

### 2.3. Modeling black hole mergers

In the final stages of a galaxy merger the dark matter halos of the galaxies merge and in the center a single stellar system is formed from the coalescence of the two stellar components. During this process a substantial fraction of the gaseous component is funneled to the center where it can drive strong starbursts and AGN activity. Presumably during this process the two central supermassive BHs form a binary, that hardens and eventually leads to a coalescence of the BHs. However, it is not clear how long this process would last and what the dominant mechanism for the hardening of the binary would be. Possible mechanisms include hardening of the BH binary through stellar-dynamical (Makino & Funato 2004; Merritt & Milosavljević 2005) and hydrodynamical (Escala et al. 2004) processes. At the final stages of the BH merger ( $d \lesssim 0.01\text{pc}$ ) gravitational radiation will dominate angular momentum and energy losses and cause the two BHs to coalesce (e.g. Flanagan & Hughes 1998). However for unequal-mass BH pairs, gravitational wave emission also removes net linear momentum and can impart a recoil velocity to the center of mass of the system. This recoil velocity is typically of the order of  $v_{\text{CM}} \sim 100 - 400 \text{ km s}^{-1}$  and may play a role in removing relatively low-mass supermassive BHs from dwarf galaxies at moderately to high redshifts (Madau & Quataert 2004; Merritt et al. 2004).

In the simulations presented in this paper we lack the required resolution to follow the hardening and eventual merging of the BHs. Using current numerical techniques it is not possible to accurately resolve the dynamical evolution of a galactic BH pair on the relevant scales, although alternative techniques such as the particle-splitting method (Mayer et al. 2007) and adaptive mesh refinement simulations (Levine et al. 2007) might allow one to follow the BH dynamics to somewhat smaller separations compared to traditional methods. Instead, as was the case for the BH accretion, we use an effective model that ensures rapid merging of the BHs once they come sufficiently close to each other. There is circumstantial evidence suggesting that the merging of BHs is efficient. If this was not the case, it should be common for a third black hole to be brought in by merger, in which case the BH binary and third BH could lead to sling-shot ejection of all three BHs (Saslaw et al. 1974). This process would seriously hamper the growth of supermassive black holes. Thus the very existence of supermassive black holes together with the relatively low number of known supermassive BH binaries (Sillanpaa et al. 1988; Merritt & Milosavljević 2005) can be taken as an indication that BH binaries typically merge efficiently. Upcoming gravitational wave experiments, such as LISA will bring more clarity to the duration and true number of BH mergers in the local Universe (Hughes 2002).

In this study we adopt the criterion of Springel et al. (2005b) for BH merging, which allows for rapid BH merging. Two BHs are assumed to merge instantly if they come within the smoothing length of each other and if their relative velocity at this time is below the local sound speed, as determined from the nearest neighbors within the SPH kernel. The momentum is conserved when gas is absorbed by the BH sink particle, thus an accreting BH moving in a gas-rich environment will experience a friction force that reduces the relative motion of the BH with respect to the surrounding gas. However, we found that

for unequal-mass mergers this description was not always adequate in ensuring rapid merging of the black holes. Typically the black holes had too large relative velocities to allow for merging and thus an alternative method had to be employed to ensure the merging of the BHs. After discussions with Volker Springel (Springel, private communication) we decided to adopt a model, in which the BH is repositioned at every time step to the minimum of the local potential. This minimum is evaluated by finding the gas particle within the SPH smoothing length of the BH which has the minimum gravitational potential. The BH is then repositioned to the location of this minimum at every timestep. This method effectively glues the BH to the center of the galaxy. Using this description the BH will remain in the merging galaxies as long as the galaxy core structure is intact. After disruption the two BHs will rapidly slide to the center of the parent galaxy and merge. Although this method is crude it should provide an adequate representation of a model, where one assumes that BH merging is very efficient once the two BHs reside in the same parent galaxy.

### 3. SIMULATIONS

#### 3.1. Galaxy models

Our progenitor galaxies are setup using the method described by Springel et al. (2005b). The virial mass and radius of each model is determined by the virial velocity  $v_{\text{vir}}$  of the halo assuming a virial overdensity of  $\Delta_{\text{vir}} = 200$  using the following relations

$$M_{\text{vir}} = \frac{v_{\text{vir}}^3}{10GH_0}, \quad (6)$$

$$r_{\text{vir}} = \frac{v_{\text{vir}}}{10GH_0}, \quad (7)$$

where  $H_0 = 71 \text{ km s}^{-1}\text{Mpc}^{-1}$  is the present day Hubble parameter. Thus  $v_{\text{vir}}$  sets the mass of the model. The virial radius together with the concentration parameter  $c = r_{\text{vir}}/r_s$  for a NFW halo (Navarro et al. 1997) is then used to construct Hernquist (1990) profile dark matter halos using the conversion detailed in Springel et al. (2005b). For all galaxy models we assume a concentration of  $c = 9$ , which is a typical value for a halo at  $z = 0$  (Bullock et al. 2001). All of our model galaxies thus correspond to local  $z = 0$  disk galaxies and unlike Robertson et al. (2006b) we do not attempt a redshift-dependent scaling of our initial conditions.

The dark matter halos are then populated with exponential disks with a constant mass fraction of  $m_d = 0.041$  of the total virial mass resulting in a total disk mass of  $M_d = m_d M_{\text{vir}}$  with a fractional gas content of  $f_{\text{gas}}$  and the rest being stars. The disk scale length  $r_d$  is determined using the Mo et al. (1998) formalism under the assumption that the fractional disk angular momentum  $j_d$  equals the disk mass fraction  $m_d$  for a constant halo spin of  $\lambda = 0.033$  for all models. This assumption of  $J_d = j_d J_{\text{halo}}$  ( $j_d = m_d$ ) corresponds to the conservation of the specific angular momentum of the material that forms the disk. The value for the spin parameter is close to the mean value found in numerical simulations (e.g. Vitvitska et al. 2002). The vertical scaleheight  $z_0$  of the stellar disk is radially constant and set to  $0.2r_d$  and the radial velocity dispersion is set to equal the vertical velocity dispersion. The vertical scale height of the gaseous

disk is set via an integral constraint on the surface mass density, a self-consistently determined galaxy potential and the effective equation of state (EOS) of the multiphase interstellar medium model (McKee & Ostriker 1977; Efstathiou 2000; Johansson & Efstathiou 2006). For the EOS we adopt the strongly pressurized multiphase model of the ISM,  $q_{\text{EOS}} = 1$  (Springel & Hernquist 2003) that allows the construction of stable galaxy models even with very large gaseous fractions (Springel et al. 2005b).

All our galaxy models include a Hernquist (1990) stellar bulge component with constant total mass fraction of  $m_b = 0.01367$  ( $M_b = m_b M_{\text{vir}}$ ), which is a third of the disk mass fraction. The bulge scale length  $b$  is also set to  $0.2r_d$ . Finally we insert a seed black hole with mass  $M_{\text{BH}} = 10^5 M_{\odot}$  at rest in the center of each galaxy model.

### 3.2. Simulation parameters

At our standard numerical resolution we set the primary galaxy models up with 20,000 gas and stellar disk particles, 10,000 bulge particles and 30,000 dark matter particles. For the secondary galaxies in 3:1 mergers we use a third of the particle resolution of the primary galaxies, thus resulting in 6,667 gas and stellar disk particles, 3,333 bulge particles and 10,000 dark matter particles. We set the gravitational softening length of gas, newly formed stars and the black hole particles to  $\epsilon = 0.1h^{-1}\text{kpc}$  and scale the softening lengths of the disk, bulge and more massive dark matter particles with the square root of the particle mass resulting in  $\epsilon = 0.2h^{-1}\text{kpc}$  for the bulge and disk particles and  $\epsilon = 0.8h^{-1}\text{kpc}$  for the dark matter particles. This ensures that the maximum gravitational force exerted from a particle is independent of its mass (Dehnen 2001). Naab et al. (2006a) also showed that small variations in the respective softening lengths have only a minor effect on the central gas content, with typically only a 10% increase in the central gas content when equal softening lengths and mass resolution were employed for all collisionless particles. The SPH properties of the gas and BH particle are averaged over the usual GADGET-2 spline SPH kernel using  $\sim 64$  SPH gas particles. Furthermore we require that the minimum SPH smoothing length is equal to the gravitational softening length. This choice safeguards against artificial stabilization of small clumps at low resolution (Bate & Burkert 1997). In order to resolve the flow of gas around the black hole accurately we ran all simulations with high force accuracy of  $\alpha_{\text{force}} = 0.005$  and time integration accuracy of  $\eta_{\text{acc}} = 0.02$  (see Springel 2005 for details).

The parameters governing the multi-phase feedback model are set as follows: The star formation timescale  $t_*^0 = 8.4$  Gyr, the cloud evaporation parameter  $A_0 = 4000$  and the supernova 'temperature'  $T_{\text{SN}} = 4.0 \times 10^8$  K that reflects the heating rate from a population of supernovae for a given IMF. Thus, we here again follow Springel et al. (2005b) who showed that these choices result in a star formation rate of  $\sim 1M_{\odot}\text{yr}^{-1}$  for a Milky Way-like galaxy. However, we note that these choices yield a comparatively low star formation rate that lies slightly below the observed Kennicutt relation (Kennicutt 1998).

We set the dimensionless efficiency parameter of accre-

TABLE 1  
ISOLATED GALAXIES AND THE  $M_{\text{BH}} - \sigma$  AND  $M_{\text{BH}} - M_*$  RELATIONS

$v_{\text{vir}}^a$	$f_{\text{gas}}$	$M_{\text{BH}}^b$	$\sigma_{\text{bulge}}^c$	$M_{\text{bulge}}^d$	$\frac{M_{\text{BH}}}{M_{\text{BH},\sigma}}^e$	$\frac{M_{\text{BH}}}{M_{\text{BH},M_*}}^f$
80	0.4	5.12	57.0	0.23	0.59	0.22
111	0.2	6.50	78.3	0.61	0.21	0.09
160	0.2	56.0	120.4	1.83	0.32	0.24
320	0.8	2640	252.9	14.7	0.76	1.08

<sup>a</sup>Virial velocity in [ $\text{kms}^{-1}$ ]

<sup>b</sup>Final mass of the BH in  $10^5 M_{\odot}$

<sup>c</sup>Final bulge stellar velocity dispersion in km/s

<sup>d</sup>Final bulge mass in  $10^{10} M_{\odot}$

<sup>e</sup>The ratio of the final BH mass to the BH mass expected from Eq. 8 if the final BH would lie on the  $M_{\text{BH}} - \sigma$  relation.

<sup>f</sup>The ratio of the final BH mass to the BH mass expected from Eq. 9 if the final BH would lie on the  $M_{\text{BH}} - M_*$  relation

tion in Eq. 1 to  $\alpha = 100$ , which is considerably higher than the theoretically expected value of  $\alpha \sim 1$ . This discrepancy is essentially due to limits imposed by the numerical resolution and the effective subresolution model for star formation. The estimated values for the gas density and thermal sound speed are large-scale averages of the gas at the location of the BH resulting in artificially low densities and high sound speeds compared to the case where the multi-phase structure of the ISM could be spatially resolved on the scale of the Bondi radius. Thus the larger value for  $\alpha$  can essentially be seen as an empirical correction factor that translates from the resolvable low mean density to the time-averaged small-scale density at the location of the BH. A similar conclusion was reached by Khalatyan et al. (2007), who set  $\alpha = 300$  in their simulations. The exact choice of  $\alpha$  within a factor of a few is not critical as long as  $\alpha$  is large enough to allow a black hole in a gas-rich environment to reach the Eddington regime, (again see Springel et al. 2005b for details). As detailed in §2.2 we set the radiative efficiency to  $\epsilon_r = 0.1$  and the thermal coupling constant of the black hole feedback energy to  $\epsilon_f = 0.05$ .

All simulations presented in this paper were evolved for a total of  $t = 3$  Gyr using the local Altix 3700 Bx2 machine hosted at the University Observatory in Munich.

### 3.3. Isolated disks with BHs

We begin by running a representative sample of our disk galaxy models in isolation in order to study the stability of the constructed galaxy models. The models are run at our standard numerical resolution. In Fig. 1 we show the resulting star formation rates, BH accretion rates and BH mass growth for four models with 20% (black), 40% (green), 80% (red) initial gas mass fractions. All galaxies show stable evolution in their star formation and BH accretion rates, reproducing the isolated disk results for a stiff EOS with  $q_{\text{EOS}} = 1$  presented by Springel et al. (2005b).

All models start with a seed black hole with mass  $M_{\text{BH}} = 10^5 M_{\odot}$  at rest in the center, which grows due to gas accretion during the simulation as is shown in the bottom panel of Fig. 1. After completing the isolated disk simulations we calculate the final black hole mass of the galaxies together with the mass-weighted line-of-sight stellar velocity dispersion  $\sigma_{\text{bulge}}$  measured from the bulge stellar particles using 50 randomly projected realizations of the galaxy models. Using the extracted velocity dispersions we then calculate the expected BH masses of the

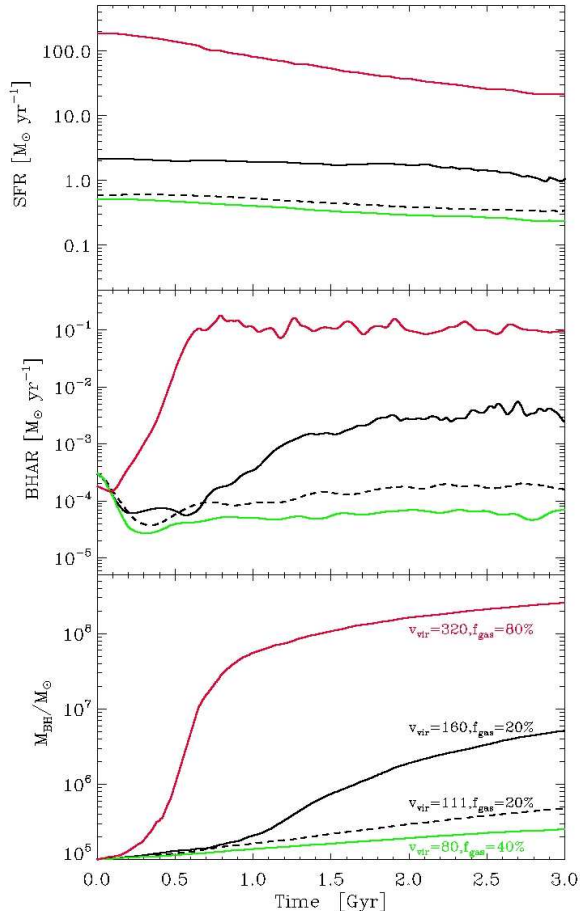


FIG. 1.— The star formation rate (top), the black hole accretion rate (middle) and the evolution of the black hole mass (bottom) as a function of time for four isolated galaxy models with initial gas mass fractions of 20% (black), 40% (green) and 80% (red) and virial velocities as indicated in the Figure.

galaxies and check if they lie on the observed  $M_{\text{BH}} - \sigma$  relation,

$$\log(M_{\text{BH}}/M_{\odot}) = a + b \log(\sigma/\sigma_0), \quad (8)$$

where the relation is defined relative to  $\sigma_0 = 200 \text{ km s}^{-1}$ . The observed values as determined by Tremaine et al. (2002) are  $a = 8.13 \pm 0.06$  for the normalization coefficient and  $b = 4.02 \pm 0.32$  for the slope. We also evaluate the total bulge stellar mass  $M_{\text{bulge}}$  by adding up the mass of all the stellar bulge particles. By definition this mass is not changing throughout the simulation, as the newly formed stars form from gas in the disk and we do not include their potential contribution to the final stellar bulge mass. We then compare the final BH masses with the expected BH masses if the galaxies would lie on the observed  $M_{\text{BH}} - M_*$  relation, where we now use  $M_*$  to denote the total bulge mass.

$$\log(M_{\text{BH}}/M_{\odot}) = c + d \log(M_*/10^{11} M_{\odot}). \quad (9)$$

The best fit observed values as determined by Häring & Rix (2004) are  $c = 8.20 \pm 0.10$  for the normalization coefficient and  $d = 1.12 \pm 0.06$  for the slope. The final BH masses, stellar velocity dispersions, final stellar masses and the ratios between the final BH mass and the BH mass derived from Eqs. 8 and 9 assuming

that the galaxies lie on the  $M_{\text{BH}} - \sigma$  and  $M_{\text{BH}} - M_*$  relations respectively are tabulated in Table 1.

The initial seed mass of  $M_{\text{BH}} = 10^5 M_{\odot}$  corresponds to a velocity dispersion of  $\sigma = 33 \text{ km s}^{-1}$  (Eq. 8), which would be the corresponding velocity dispersion of a galaxy with  $v_{\text{vir}} \sim 50 \text{ km s}^{-1}$ . Thus the BHs of the galaxies are not initially on the  $M_{\text{BH}} - \sigma$  relation, but evolve towards this relation during the simulation. The bulge velocity dispersions of the galaxies only increase slightly on the  $\sim 10\%$  level during the simulations. The governing factor determining the evolution of the BHs for the isolated disk galaxies is the depth of the potential well and the gas mass fraction. This can be seen in the ratio of the final BH mass to the expected BH mass from Eq. 8 tabulated in Table 1. The lower the gas mass fraction the lower the final BH masses are with respect to the expected  $M_{\text{BH}} - \sigma$  relation. Models with lower gas mass fractions would require additional gas inflow to the central regions in order to ensure sufficient BH growth. Such additional gas inflow could be triggered by galaxy mergers. The same initial BH seed mass of  $M_{\text{BH}} = 10^5 M_{\odot}$  would require initially a total bulge mass of  $M_* = 1.4 \cdot 10^8 M_{\odot}$ . Again this would only be valid for the very lowest mass initial galaxy models and thus generally the galaxies do not initially lie on the  $M_{\text{BH}} - M_*$  relation. Typically the simulations of the isolated galaxies result in BH masses that are too low for their given stellar bulge masses. Again an additional central gas flow, potentially induced by a galaxy merger is required for the central BHs to reach the masses expected by their corresponding stellar bulge masses.

Interestingly the simulation of the most massive and gas-rich galaxy (the  $f_{\text{gas}} = 80\%$ ,  $v_{\text{vir}} \sim 320 \text{ km s}^{-1}$  model in Fig. 1 and Table 1) results in a final BH mass that is relatively close to the BH mass expected from the  $M_{\text{BH}} - \sigma$  relation and even superceeds the BH mass expected from the  $M_{\text{BH}} - M_*$  relation. However, some of this BH mass growth may be artificially high, due to the fact that the current BH feedback model does not restrict the size of the BH accretion radius. Thus the accretion radius of a massive BH in a gas-rich region may grow to unphysically large sizes and accrete material that would physically not end up in the BH because of its high angular momentum and large distance from the BH. This is typically not a problem in merger simulations, where most of the BH mass grows by accretion of nearby high-density gas.

#### 3.4. The effect of resolution on the $M_{\text{BH}} - \sigma$ relation

We then proceed with a detailed analysis of the effect of the BH merger prescription and resolution on the final mass of BHs and the corresponding stellar velocity dispersions in 3:1 and 1:1 merger remnants. We simulate 3:1 mergers with a quarter (tiny), half (low), double (medium) and four times (high) the number of particles compared to our standard numerical resolution (§3.2). In addition we compute a control sample of 1:1 mergers at the standard, low and tiny resolutions. The five 3:1 and three 1:1 initial conditions are simulated using both the standard BH merging prescription and the BH repositioning method described in §2.3 resulting in a total of 16 simulations (see Table 2 for details). The gravitational softening lengths for all the particles including the BH are scaled with the inverse cube root of the number

TABLE 2  
 3:1 AND 1:1 BINARY BH MERGER RESOLUTION AND MERGER PRESCRIPTION STUDY

Resolution <sup>a</sup>	Mass ratio	$\epsilon_{\text{gas}}^{bc}$	$\epsilon_{\text{disk}}^d$	$\epsilon_{\text{DM}}$	$N_{\text{gas}}^e$	$N_{\text{bulge}}$	$N_{\text{DM}}$	$m_{\text{gas}}^f$	$M_{\text{BH,fin}}^g$	$\sigma_{\text{fin}}^h$	$t_{\text{merg}}^i$
Tiny Std	3:1	0.16	0.32	1.28	5000	2500	7500	31	46.0	136.9	2.02
Tiny Repos	3:1	0.16	0.32	1.28	5000	2500	7500	31	118	132.2	2.81
Low Std	3:1	0.125	0.25	1.00	10000	5000	15000	15.5	57.0	134.4	2.00
Low Repos	3:1	0.125	0.25	1.00	10000	5000	15000	15.5	118	127.7	2.50
Standard Std	3:1	0.1	0.2	0.8	20000	10000	30000	7.75	81.7	134.7	—
Standard Repos	3:1	0.1	0.2	0.8	20000	10000	30000	7.75	126	126.8	1.82
Medium Std	3:1	0.08	0.16	0.64	40000	20000	60000	3.87	26.7	133.5	1.84
Medium Repos	3:1	0.08	0.16	0.64	40000	20000	60000	3.87	96.9	120.3	1.72
High Std	3:1	0.0625	0.125	0.5	80000	40000	120000	1.94	26.1	129.8	2.81
High Repos	3:1	0.0625	0.125	0.5	80000	40000	120000	1.94	54.2	129.5	1.86
Tiny Std	1:1	0.16	0.32	1.28	5000	2500	7500	31	420	155.4	2.21
Tiny Repos	1:1	0.16	0.32	1.28	5000	2500	7500	31	508	150.7	1.57
Low Std	1:1	0.125	0.25	1.00	10000	5000	15000	15.5	134	175.4	1.84
Low Repos	1:1	0.125	0.25	1.00	10000	5000	15000	15.5	469	153.1	1.57
Standard Std	1:1	0.1	0.2	0.8	20000	10000	30000	7.75	456	155.8	1.72
Standard Repos	1:1	0.1	0.2	0.8	20000	10000	30000	7.75	516	157.9	1.50

<sup>a</sup>The secondary has a third of the particles of the primary

<sup>b</sup>Gravitational softening lengths in  $h^{-1}\text{kpc}$

<sup>c</sup> $\epsilon_{\text{gas}} = \epsilon_{\text{stars}} = \epsilon_{\text{BH}}$

<sup>d</sup> $\epsilon_{\text{disk}} = \epsilon_{\text{bulge}}$

<sup>e</sup> $N_{\text{gas}} = N_{\text{disk}}$

<sup>f</sup>Mass of a gas particle in  $10^5 M_{\odot}$

<sup>g</sup>Final mass of the BH in  $10^5 M_{\odot}$

<sup>h</sup>Final stellar velocity dispersion within  $r_{\text{eff}}$  in km/s

<sup>i</sup>Time of BH merger in Gyr

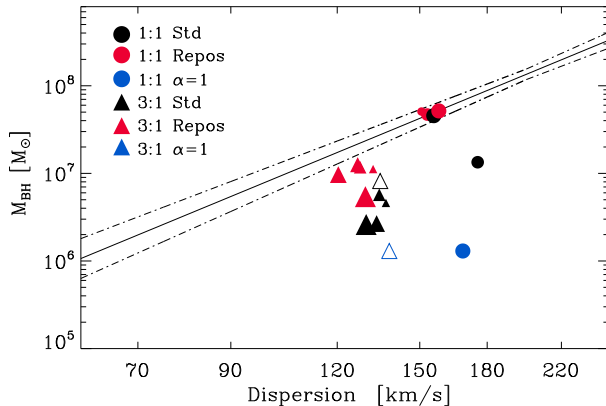


FIG. 2.— The  $M_{\text{BH}} - \sigma$  relation as a function of resolution and merger prescription, with larger/smaller symbols indicating higher/lower resolution, respectively (Table 2). Triangles show 3:1 and circles 1:1 merger remnants. Black symbols employ the standard merger prescription and the red symbols use the BH repositioning method. The blue symbols also employ the BH repositioning method but with a reduced accretion efficiency of  $\alpha = 1$ . The solid/open symbols indicate cases where the BHs did/did not merge. (Table 2). The lines show the observed relation with errors by Tremaine et al. (2002).

of particles, with larger numerical resolution resulting in smaller gravitational softening lengths. In addition we run a 3:1 and a 1:1 merger with a lower accretion efficiency of  $\alpha = 1$  at our standard resolution using the BH repositioning method.

All galaxy models have a 20% initial gas fraction, with  $v_{\text{vir,p}} = 160 \text{ km s}^{-1}$ ,  $v_{\text{vir,s}} = 111 \text{ km s}^{-1}$  and are setup with the parameters described in §3.1 (p and s denote the primary and secondary galaxies, respectively). In order to isolate the effects of resolution and merging prescription all 3:1 and 1:1 mergers are run with identical merging geometries and initial disk orientations. For the orbit

and initial orientation we adopt geometry G13 for both the 3:1 mergers and 1:1 mergers from Naab & Burkert (2003). The G13 geometry corresponds to the inclinations  $i_p = -109$ ,  $i_s = 180$  and the arguments of the pericenter  $\omega_p = 60$ ,  $\omega_s = 0$  for the primary and secondary galaxies, respectively. The galaxies approach each other on a parabolic orbit where the initial separation of the progenitors is  $R_{\text{init}} = 0.5(r_{\text{vir,p}} + r_{\text{vir,s}})$  and the pericentric distance is  $r_{\text{peri}} = r_{\text{d,p}} + r_{\text{d,s}}$ , where  $r_{\text{vir,p}}$ ,  $r_{\text{d,p}}$  and  $r_{\text{vir,s}}$ ,  $r_{\text{d,s}}$  are the virial and disk scale radii for the primary and secondary galaxies, respectively. We note that radial parabolic or near-parabolic orbits are generally motivated by statistics from N-body simulations (Khochfar & Burkert 2006).

After completing the merger simulations we calculate the final black hole mass together with mass-weighted line-of-sight stellar velocity dispersion  $\sigma$  measured from all stellar particles within the projected half-mass radius  $r_e$  using 50 randomly projected realizations of the merger remnant. This determination of  $\sigma$  is similar to the method used by observers who measure the luminosity-weighted velocity dispersion within an effective radius (Gebhardt et al. 2000). The simulated final BH masses and stellar velocity dispersions together with the time of the BH merger are tabulated in Table 2.

For the 3:1 mergers, the merging prescription has a strong effect on the final BH mass of the merger remnant, with the standard prescription producing BH masses that are a factor of 2-3 lower than the corresponding BH masses using the repositioning method. The final stellar velocity dispersion on the other hand converges with increasing resolution, with the repositioning method resulting in marginally lower velocity dispersions. The 3:1 mergers with the standard BH merger prescription result in BH masses that are too low for their corresponding velocity dispersions as shown in Fig. 2, where the simulated 3:1 (triangles) and 1:1 (circles) results are over-

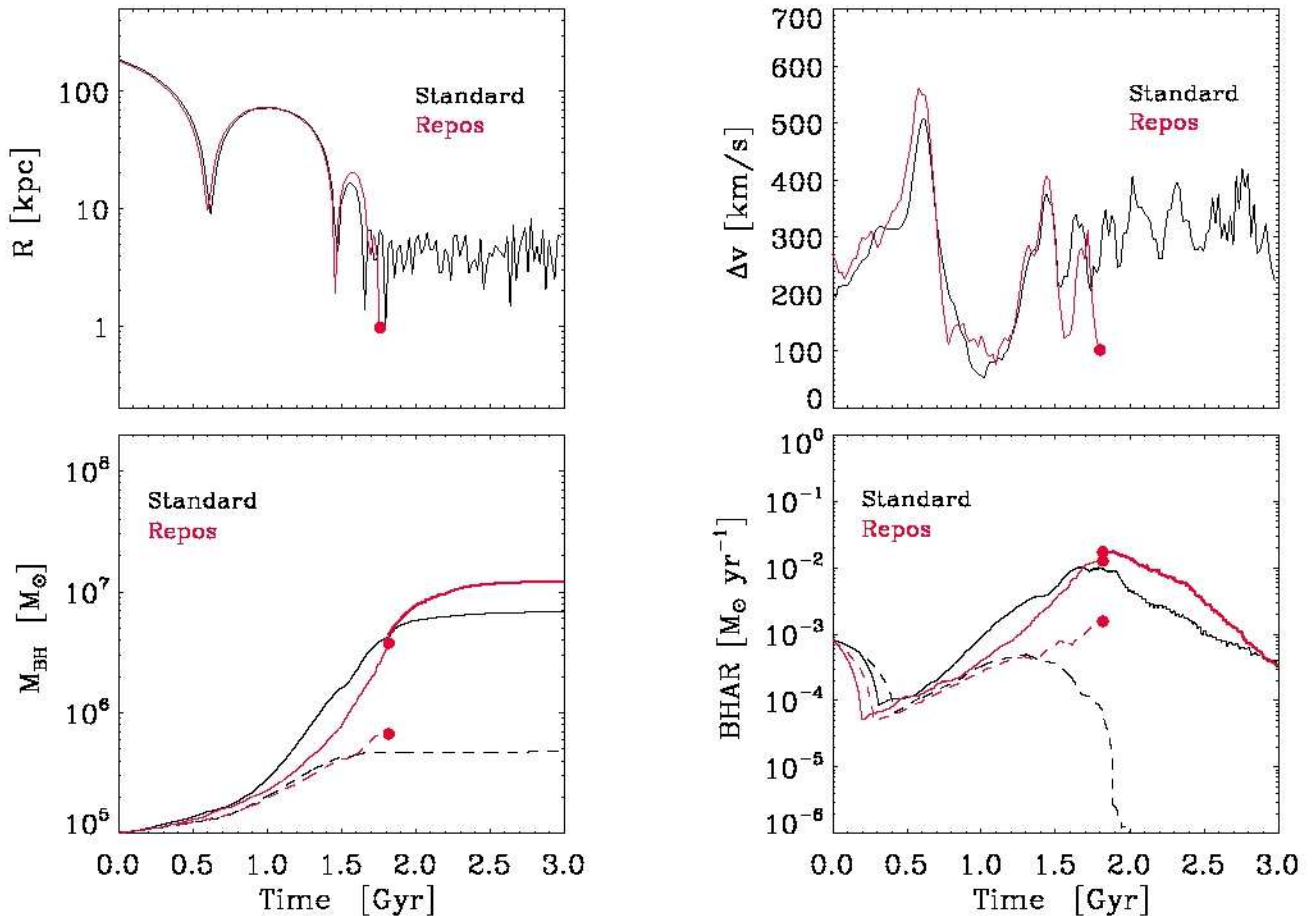


FIG. 3.— 3:1 unequal-mass merger simulations run at the standard numerical resolution with the standard BH merger prescription (black lines) and the repositioning method (red lines). The top left and right panels show the relative distances and velocities between the BHs as a function of time. The bottom panels show the evolution of the BH masses and accretion rates as a function of time. The solid line depicts the primary BH, the dashed line the secondary BH and the thick solid line the merged BH, with the time of merging indicated with solid circles.

plotted on the observed  $M_{\text{BH}} - \sigma$  relation from Eq. 8 by Tremaine et al. (2002).

For the 1:1 mergers the effect of the merger prescription is less pronounced. With the exception of a single simulation at low resolution, all 1:1 mergers result in very similar BH masses and velocity dispersions. At the standard resolution the two prescriptions produce final BH masses and velocity dispersions that agree within 10% with each other and the observed relation. All the 1:1 mergers with repositioning and two out of three of the standard prescription mergers lie on the observed  $M_{\text{BH}} - \sigma$  relation as shown in Fig. 2.

Finally we show that reducing the accretion efficiency from our standard value of  $\alpha = 100$  to the physically motivated  $\alpha = 1$  produces BH masses that are far too low for their corresponding velocity dispersions (the blue points in Fig. 2). However, this is expected given the limitations imposed by the numerical resolution and sub-resolution modeling as was discussed in §3.2. Changing the accretion efficiency or even removing the BH altogether does not affect the final stellar velocity dispersion, which is primarily set by the depth of the potential well. Thus, this implies that the BH is not dynamically important for the galaxy as a whole. A similar problem would arise when comparing the simulated BH masses

to the total stellar masses of the galaxies. Variations in numerical resolution and BH merging prescription affect only marginally the star formation rate and thus the BH masses in the standard prescription 3:1 merger remnants would be too low compared to their corresponding stellar masses.

### 3.5. Merger prescription and resolution studies

In order to explore the discrepancy between the two BH merger prescriptions in more detail we plot in Fig. 3 the black hole mass growth and mass accretion rate together with the distance and relative velocity between the black holes for our standard resolution unequal-mass 3:1 merger using both merger prescriptions. The galaxies go through their first and second passages at  $t_1 = 0.6$  Gyr and  $t_2 = 1.4$  Gyr respectively. The galaxies then approach each other for a third time at  $t_3 = 1.8$  Gyr at which time the BHs in the simulation with BH repositioning merge, unlike the standard case in which the BHs do not merge. The mass growth of both the primary (solid lines) and the secondary (dashed lines) BHs are similar for both methods until the merger, after which time essentially only the repositioned BH grows in mass. A similar result can be seen in the BH accretion rates, which are similar until  $t_3 = 1.8$  Gyr, after which the repositioned BH shows almost an order of magnitude higher accretion

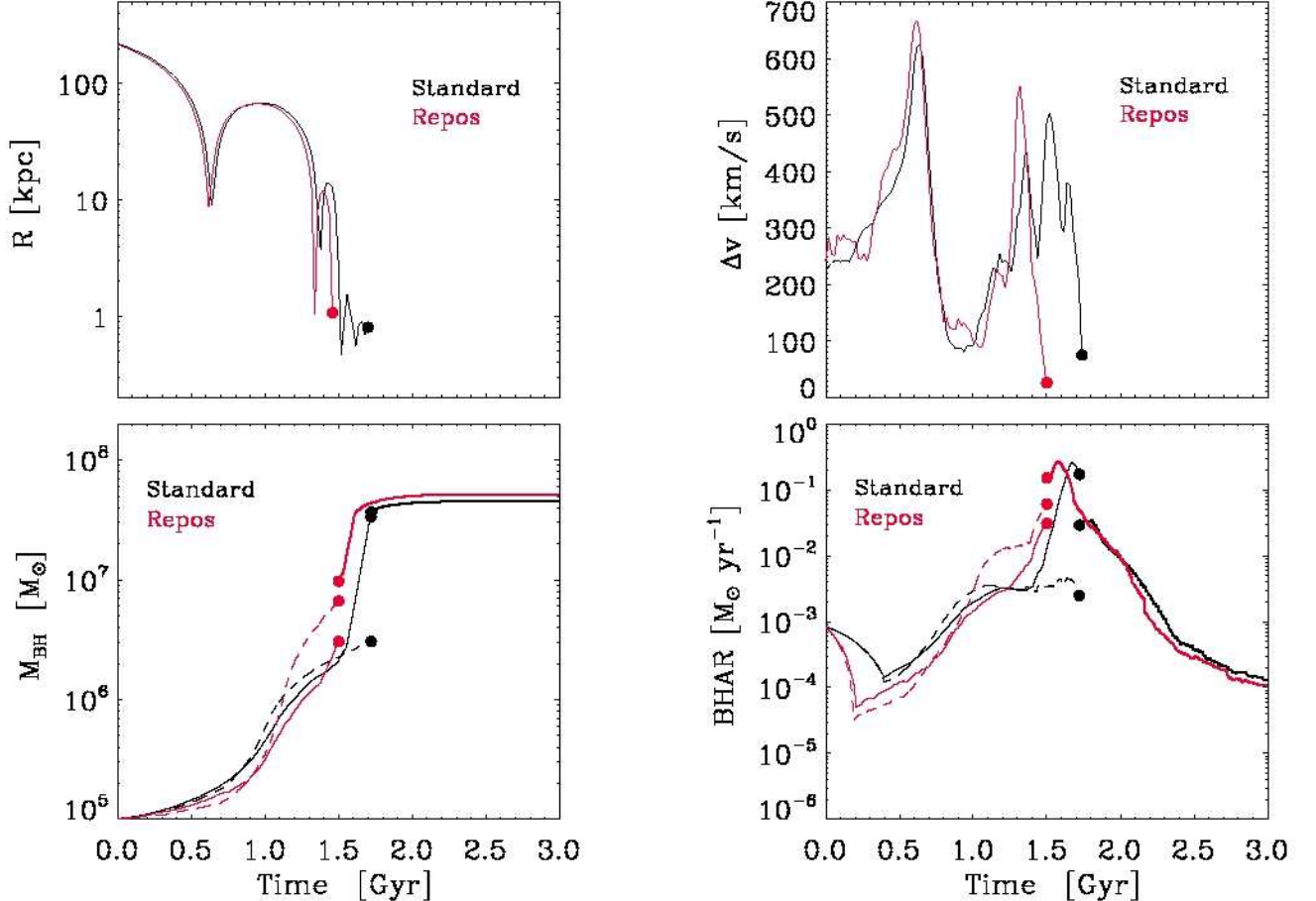


FIG. 4.— 1:1 equal-mass merger simulations run at the standard numerical resolution with the standard BH merger prescription (black lines) and the repositioning method (red lines). The top left and right panels shows the relative distances and velocities between the BHs as a function of time. The bottom panels show the evolution of the BH masses and accretion rates as a function of time. The solid line depicts the primary BH, the dashed line the secondary BH and the thick solid line the merged BH, with the time of merging indicated with solid circles.

rates compared to the standard BH merger case. One can also see that the secondary BH mass accretion rate dramatically drops at this time, hence terminating the growth of the secondary BH. This is caused by the fact that the secondary BH is perturbed away from its surrounding gas disk during the final stages of the merger.

In the standard BH merger prescription the merging of the BHs is typically delayed with respect to the BHs in the repositioning runs. During the BH merger the momentum is conserved, which can give the BH a relatively large ‘kick’, especially in the 3:1 mergers where the mass ratio of the BHs is relatively large. The repositioning ensures that after the merger the BH quickly resettles in the center of the central gas disk that is feeding the BH. In the standard prescription the merged BH remains longer displaced from the central gas disk, thus lowering the mass accretion rate, which scales linearly with density ( $\dot{M}_B \propto \rho$  in Eq. 1). The repositioning also lowers the relative velocity of the BH with respect to the surrounding gas. For the standard merging case the relative velocity can be relatively large with the BH plunging through the central gaseous disk. This also affects the BH accretion rate as it scales as the inverse third power of the relative BH-gas velocity for a fixed sound speed of the medium ( $\dot{M}_B \propto v^{-3}$  in Eq. 1). Finally the

BH accretion rate scales with the square of the BH mass ( $\dot{M}_B \propto M_{\text{BH}}^2$  in Eq. 1) resulting in higher accretion rates for more massive BHs, thus an earlier merging of the BHs produces typically larger final BH masses.

In Fig. 4 we plot the corresponding details for a 1:1 merger at our standard numerical resolution using the two merging prescriptions. The differences between the merger prescriptions compared to the 3:1 merger are less pronounced with the BHs merging slightly earlier in the repositioned simulation. However, the growth of the black hole masses show differences with the BHs in the repositioned run showing roughly equal mass growth prior to the BH merging compared to the standard case, where the more massive BH is an order of magnitude more massive than the secondary BH at the time of the BH merger. In the standard merging case the secondary BH is perturbed away from its gaseous central disk prior to the final merger, thus lowering the accretion rate and growth of the BH in comparison to the primary BH. After the merger the repositioned BH exhibits strong growth in a gas-rich environment until the thermal feedback energy input is large enough to clear away the remaining gas, thus terminating the BH growth. This is not mirrored in the standard merging case, where the primary BH grows strongly prior to merging and only modestly

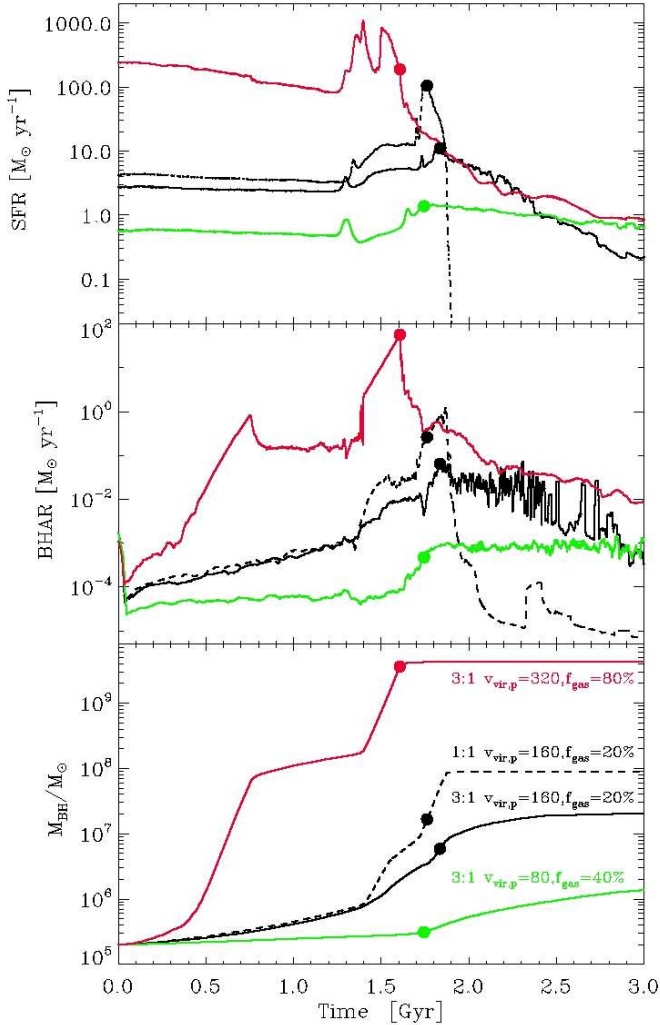


FIG. 5.— The total star formation rate (top), the total black hole accretion rate (middle) and the evolution of the total black hole mass (bottom) as a function of time for three 3:1 (solid lines) and one 1:1 (dashed line) merger with initial gas mass fractions of 20% (black), 40% (green) and 80% (red). The filled circles indicate the time of merging of the BHs.

after the merger due to the fact that the merged BH is unable to resettle in the remaining central gas disk. However, the end result of both merging prescriptions is a final BH mass and stellar velocity dispersion that agree with each other on the 10% level.

Taken together these results show that repositioning the BHs produce converged and stable results for the mass growth and accretion rates of the BHs. Repositioning is essential in representing the evolution of BHs in 3:1 mergers and also produces converged results for 1:1 mergers even at relatively low numerical resolution. The numerical resolution tests show that the central stellar velocity dispersion converge within 10% with increasing resolution, whereas the BH mass converges within 25%, with the exception of the highest resolution simulation using the repositioning method. The highest resolution reposition run produces a BH mass, which is lower by a factor of two compared to the other simulations. This is mainly due to the reduction of the gravitational softening of the BH particle. The accretion rate and mass growth

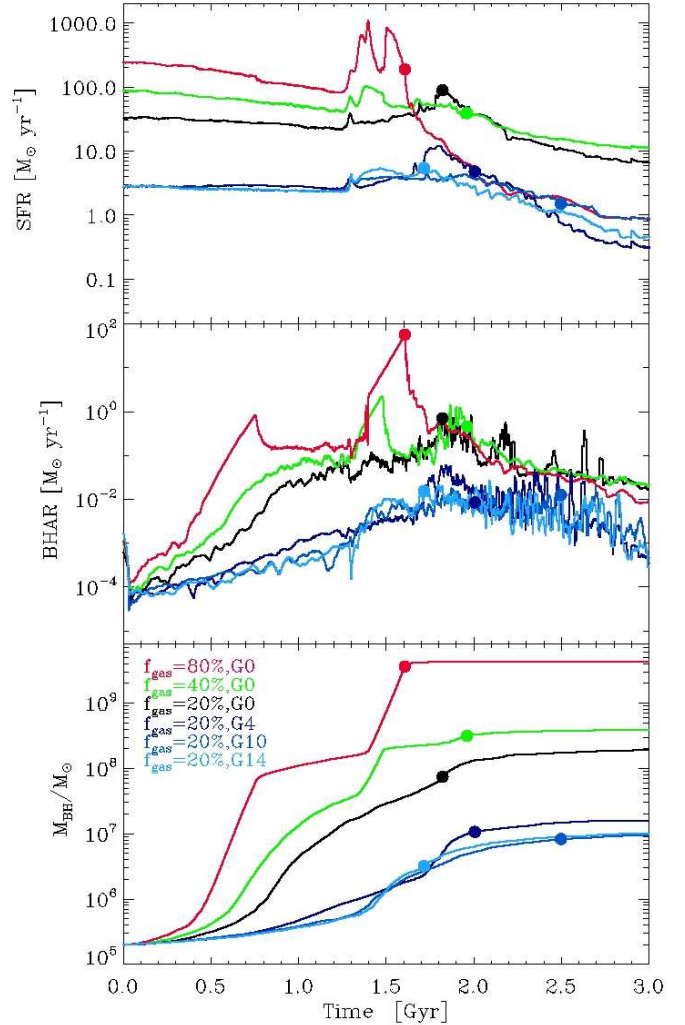


FIG. 6.— The total star formation rate (top), the total black hole accretion rate (middle) and the evolution of the total black hole mass (bottom) as a function of time for three 3:1 mergers with varying initial gas mass fractions (black, green, red lines) and three 3:1 mergers with varying orbital and initial geometries for a fixed gas fraction (blue lines).

of the BH is determined by a combination of the accretion efficiency ( $\alpha$  in Eq. 1) and the gravitational softening. Our chosen value of accretion efficiency was adopted for our standard numerical resolution, thus it is not surprising that smaller gravitational softening lengths produce slightly smaller BH masses. We conclude that the repositioning merger prescription at the standard numerical resolution produces stable results for both 3:1 and 1:1 binary galaxy mergers with BHs. Thus we adopt this prescription and numerical resolution for all remaining simulations presented in this paper.

## 4. RESULTS

### 4.1. Unequal-mass 3:1 disk mergers with BHs

Using the galaxy models described in §3.1 we set up five unequal-mass 3:1 mergers and five equal-mass 1:1 mergers with three different initial gas mass fractions of  $f_{\text{gas}} = 0.2, 0.4, 0.8$ , resulting in a total of thirty simulations (the S1- and S2-series in Table 3). The progenitor galaxies are at the standard numerical resolu-

TABLE 3  
 UNEQUAL- AND EQUAL-MASS MERGERS

Models	$v_{\text{vir,prog1}}^a$	$v_{\text{vir,prog2}}$	Mass ratio	Orbit	$f_{\text{gas}}$	$N_{\text{gas,tot}}^b$	$N_{\text{bulge,tot}}$	$N_{\text{DM,tot}}$	$N_{\text{sim}}$
S1-1:1	50, 80, 160, 320, 500	50, 80, 160, 320, 500	1:1	G0	0.2, 0.4, 0.8	40000	20000	60000	15
S2-3:1	50, 80, 160, 320, 500	35, 55, 111, 222, 347	3:1	G0	0.2, 0.4, 0.8	26667	13333	40000	15
G1-1:1	160	160	1:1	G7, G10, G13	0.2	40000	20000	60000	3
G2-3:1	160	111	3:1	G4, G10, G14	0.2	26667	13333	40000	3

<sup>a</sup>All virial velocities in  $\text{kms}^{-1}$

<sup>b</sup> $N_{\text{gas}} = N_{\text{disk}}$

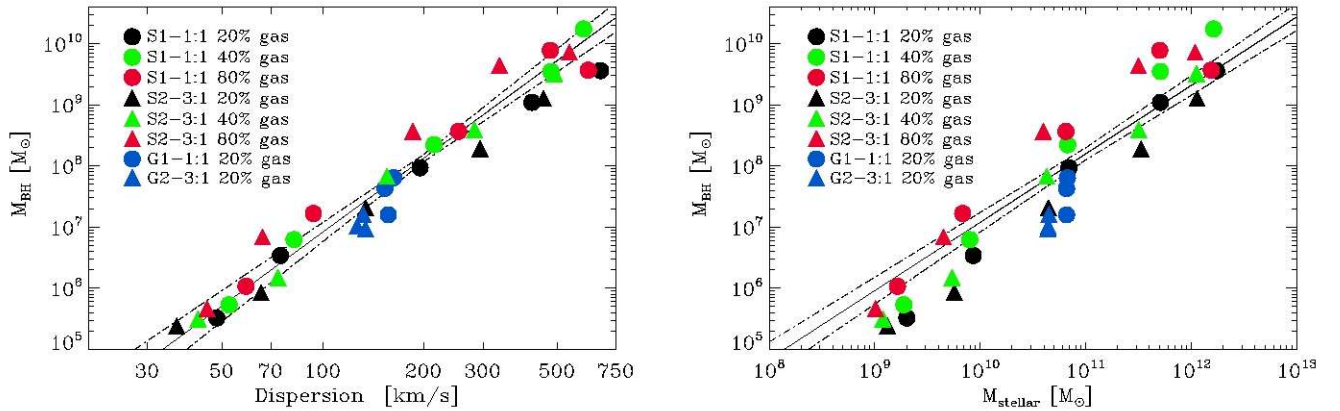


FIG. 7.— The  $M_{\text{BH}} - \sigma$  (left) and  $M_{\text{BH}} - M_*$  (right) relations for our complete sample of 3:1 (triangles) and 1:1 (circles) mergers. The black, green and red symbols show the effect of varying the initial gas mass fraction for our S1- (equal-mass) and S2-samples (unequal-mass). The blue symbols show the variation caused by the orbit and initial geometry for our G1- and G2-samples (see also Table 3). The lines show the observed relations with errors by Tremaine et al. (2002) (left panel) and Häring & Rix (2004) (right panel), respectively.

TABLE 4  
 BEST FIT  $M_{\text{BH}} - \sigma$  RELATION FOR 3:1 AND 1:1 MERGERS

Sample	N	$a$	$b$	$\Delta_{\log M_{\text{BH}}}$
Tot sample	36	$8.07 \pm 0.06$	$3.82 \pm 0.15$	0.29
3:1 sample	18	$8.06 \pm 0.08$	$3.78 \pm 0.18$	0.33
1:1 sample	18	$8.05 \pm 0.07$	$3.77 \pm 0.18$	0.26
S1-S2 20% gas sample	10	$7.85 \pm 0.04$	$3.47 \pm 0.12$	0.13
S1-S2 40% gas sample	10	$8.13 \pm 0.05$	$3.96 \pm 0.13$	0.14
S1-S2 80% gas sample	10	$8.35 \pm 0.10$	$3.77 \pm 0.28$	0.29
Observed sample <sup>a</sup>	31	$8.13 \pm 0.06$	$4.02 \pm 0.32$	0.25-0.3

<sup>a</sup>From Tremaine et al. (2002).

tion with the virial velocities of the models ranging from  $v_{\text{vir,p}} = 50 - 500 \text{ kms}^{-1}$  and  $v_{\text{vir,s}} = 35 - 347 \text{ kms}^{-1}$  for the primary and secondary galaxies, respectively. The progenitors merge on prograde, nearly parabolic, in plane orbits (G0 orbit), with inclinations  $i_1 = i_2 = 0$  and arguments of the pericenter  $\omega_1 = \omega_2 = 0$ . The initial separation and pericentric distances are set to the mean of the virial radius and twice the mean of the scale radius respectively, as detailed in §3.4. In addition we simulate a set of three 3:1 and three 1:1 mergers with varying initial disk geometries and orbits. These simulations (the G1- and G2-series in Table 3) were all run with  $f_{\text{gas}} = 0.2$  and  $v_{\text{vir,p}} = 160 \text{ kms}^{-1}$ ,  $v_{\text{vir,s}} = 111 \text{ kms}^{-1}$  progenitors on the G7, G10, G13 orbits for the equal-mass mergers and the G4, G10, G14 orbits for the unequal-mass mergers (see Naab & Burkert 2003 for a definition of the orbital parameters). The orbits in the G-series were chosen to provide a good coverage of the expected anisotropy-ellipticity ( $\delta - \epsilon$ ) plane for merger remnants (see Burkert et al. 2007 for definitions of  $\delta$  and  $\epsilon$ ).

In Fig. 5 we plot the total star formation rates, BH ac-

cretion rates and the BH mass growth for three 3:1 mergers (solid lines) with 20% (black), 40% (green), 80% (red) initial gas mass fractions together with one 20% gas fraction 1:1 merger (dashed lines). The star formation is very efficiently terminated by the BH feedback in 1:1 mergers, compared to a generally much shallower decline in star formation for 3:1 mergers. In the lowest mass 3:1 merger the BH feedback is actually unable to terminate the star formation and the galaxy is forming stars at a constant rate even after the BH merger. A similar trend is true for the BH accretion rates, with a much gentler decline in the accretion rate for galaxies undergoing 3:1 mergers compared to 1:1 mergers. This evolution is mirrored in the growth of the BH masses, with the final BH mass being lower in 3:1 mergers typically by a factor of 2-5, but with a relatively large scatter depending on the progenitor masses and initial gas fractions. Most of the mass growth of the BHs typically takes place shortly after the merging of the BHs as indicated by the filled circles in Fig. 5.

In Fig. 6 we show the results for three 3:1 mergers with varying initial gas mass fractions for a fixed orbit and initial disk geometry (black, green, red lines) and for three 3:1 mergers with varying initial orbits and orientations for a fixed gas mass fraction (blue lines). The initial gas fraction has a large effect on the height of the star formation and BH accretion peaks, with larger initial gas fractions producing higher values, as expected. This results also in relatively large differences in the final BH masses, with the  $f_{\text{gas}} = 0.8$  simulations producing final BH masses that are larger by an order of magnitude compared to the  $f_{\text{gas}} = 0.2$  runs. The variation of the orbit and initial geometry for a fixed gas mass fraction

produces much smaller differences. The peaks of the star formation rates and BH accretion rates only vary within a factor of two with changing orbits and initial disk geometries. And although the time of the BH merging varies somewhat between different geometries the final BH mass is virtually unchanged. This was already shown to be the case for 1:1 mergers by Springel et al. (2005b) and Fig. 6 confirms the same conclusion for 3:1 mergers. Hence the final BH mass is sensitive to the initial gas mass fraction of the galaxies, but relatively insensitive to the initial orbit and orientation of the galaxies.

Figure 7 shows the  $M_{\text{BH}} - \sigma$  (left panel) and  $M_{\text{BH}} - M_*$  (right panel) relations, extracted from our total sample of 36 simulated mergers, with the filled triangles and circles depicting 3:1 and 1:1 merger remnants, respectively, together with the observed relations by Tremaine et al. (2002) and Häring & Rix (2004). We perform a Levenberg-Marquardt least-squares fit to the  $M_{\text{BH}} - \sigma$  relation as defined in Eq. 8. Table 4 lists the best fit values for the normalization coefficient  $a$  and the slope  $b$  together with their  $1\sigma$  uncertainties derived using the Bootstrap method. In addition we list the dispersion  $\Delta_{\log M_{\text{BH}}}$  about each best-fit relation. The fitting analysis was performed for our total merger sample, for the 3:1 and 1:1 samples separately and for the sample split as a function of the initial gas mass fraction. Our best fit normalization coefficient and slopes for the total sample are marginally lower compared to the observational values of Tremaine et al. (2002), but still well within the error limits. Furthermore the intrinsic  $M_{\text{BH}} - \sigma$  dispersion induced primarily by varying the initial gas fraction is in good agreement with the observed dispersion of  $\Delta_{\log M_{\text{BH}}} = 0.25 - 0.3$ . We also note that our results are in good agreement with the  $z = 0$   $M_{\text{BH}} - \sigma$  relation derived by Robertson et al. (2006b). We do not find any statistically significant difference between the 3:1, 1:1 and the complete merger sample, with all three samples resulting in virtually the same normalization coefficients and slopes for the  $M_{\text{BH}} - \sigma$  relation. The normalization coefficient steadily increases with increasing initial gas mass fraction. The dispersion within a sample with constant gas mass fraction is in general low, with the exception of the sample with the largest gas mass fraction. This can be taken as a further indication that the dispersion in the  $M_{\text{BH}} - \sigma$  relation is primarily driven by changing initial gas mass fractions. We conclude that the simulated  $M_{\text{BH}} - \sigma$  relation is overall robust and in agreement with the observed relation over a wide range of progenitor masses and initial gas fractions for both equal- and unequal-mass disk mergers.

Similarly, we perform a least-squares fit to the  $M_{\text{BH}} - M_*$  relation as defined in Eq. 9, with the best fit parameters, parameter errors and dispersions for our samples listed in Table 5. We here define  $M_*$  as the total mass of all luminous particles within the effective radius  $r_e$ , including disk, bulge and newly formed stellar particles. This definition assumes that the merger remnant is a pure bulge system within this radius. For equal-mass mergers this is a valid assumption, whereas for higher mass ratio mergers this method might induce some additional scatter due to an underlying surviving disk component in the final merger remnant (Naab & Trujillo 2006). In addition, we found that this definition for  $M_*$  correlates reasonably well with total bulge mass as defined by

TABLE 5  
BEST FIT  $M_{\text{BH}} - M_*$  RELATION FOR 3:1 AND 1:1 MERGERS

Tot sample	36	$8.17 \pm 0.10$	$1.40 \pm 0.07$	0.44	
3:1 sample	18	$8.04 \pm 0.11$	$1.34 \pm 0.08$	0.47	
1:1 sample	18	$8.24 \pm 0.10$	$1.41 \pm 0.10$	0.38	
S1-S2 20% gas sample	10	$7.86 \pm 0.07$	$1.34 \pm 0.05$	0.17	
S1-S2 40% gas sample	10	$8.28 \pm 0.08$	$1.45 \pm 0.06$	0.22	
S1-S2 80% gas sample	10	$8.68 \pm 0.13$	$1.36 \pm 0.12$	0.29	
Observed sample <sup>a</sup>	30	$8.20 \pm 0.10$	$1.12 \pm 0.06$	0.30	

<sup>a</sup>From Häring & Rix (2004).

the stellar bulge particles. Furthermore, this definition for  $M_*$  is similar to the one employed by Di Matteo et al. (2007); Sijacki et al. (2007) and allows us to directly compare our results to theirs. Thus we adopt the simple definition of the total stellar mass within the effective radius as a proxy for the total bulge mass for all subsequent measurements of  $M_*$ . The best fit value of the normalization coefficient ( $c$ ) for our total sample is in excellent agreement with the observations, but the derived slope  $d$  is too steep compared to the observed sample. The too large value of the slope is a general problem in all our simulation samples as can be seen in Fig. 7. For low-mass stellar systems the simulations typically produce too low BH masses, whereas for the higher-mass stellar systems the BH mass is slightly overpredicted, thus producing a tilt in the simulated relation with respect to the observed relation. The derived dispersion in the simulated relation is marginally higher than the observed scatter, with the scatter being again primarily driven by variations in the initial gas mass fraction. Interestingly the final luminous mass within the effective radius remains virtually constant with changing initial gas mass fraction. In higher gas mass fraction simulations the lower initial stellar disk mass is compensated by higher star formation rates resulting in roughly the same final stellar mass. On the other hand, higher initial gas mass fractions produce larger final BH masses, thus resulting in vertical scatter in the  $M_{\text{BH}} - M_*$  relation as can be seen in Fig. 7. This also results in a systematic increase in the normalization coefficient with increasing gas mass fraction, with the slope remaining relatively constant. A plausible explanation for the discrepancy between the simulated and observed slopes of the  $M_{\text{BH}} - M_*$  relation lies in the employed stellar feedback model. A more aggressive stellar feedback including galactic winds (Springel & Hernquist 2003; Oppenheimer & Davé 2006) would primarily affect the low-mass stellar systems, reducing their final stellar mass, thus lowering the simulated slope and bringing it in better agreement with the observed slope. Indeed, both the cosmological studies by Di Matteo et al. (2007); Sijacki et al. (2007) found a better fit to the expected relations at the low mass end when they included a model for supernova-driven galactic winds in their simulations. Given these limitations in the stellar feedback model employed in our simulations we find that the final fit to the  $M_{\text{BH}} - M_*$  relation is adequate, with a well defined normalization and a slightly steeper slope compared to the observational relation.

#### 4.2. The accretion history of BHs in unequal mergers

We now proceed to study the BH accretion and star formation histories for unequal-mass mergers with varying mass ratios. To this end we ran five mergers with

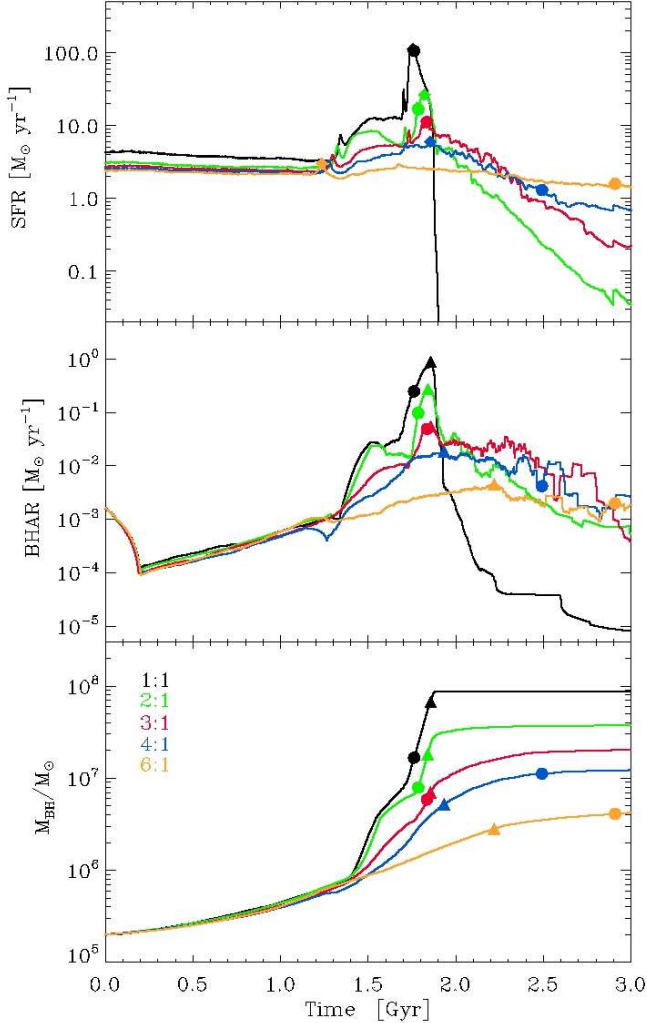


FIG. 8.— The total star formation rate (top), the total black hole accretion rate (middle) and the evolution of the total black hole mass (bottom) as a function of time for co-planar prograde (G0) 1:1 (black), 2:1 (green), 3:1 (red), 4:1 (blue) and 6:1 (orange) mergers. The filled circles indicate the time of the BH merger, the filled diamonds in the top panel and the filled triangles in the bottom two panels show the location of the maximum star formation and BH accretion peaks, respectively.

mass ratios of 1:1, 2:1, 3:1, 4:1 and 6:1 on co-planar prograde orbits (G0). This orbital configuration was chosen in order to maximize the non-axisymmetric torques during the merger resulting in the most intensive bursts in BH accretion and star formation activity (Cox et al. 2008). All the progenitor galaxies had initial gas mass fractions of 20% with the primary progenitor having  $v_{\text{vir}} = 160 \text{ km s}^{-1}$  at the standard numerical resolution. The secondary galaxies were scaled down in mass and numerical resolution accordingly in order to maintain equal mass resolution per particle. The initial seed BH mass was set to  $M_{\text{BH,init}} = 10^5 M_{\odot}$  for all models. Again, the initial separation and pericentric distances are set to the mean of the virial radius and twice the mean of the scale radius respectively as detailed in §3.4.

In Fig. 8 we show the evolution of the resulting star formation (top), BH accretion (middle) and BH mass (bottom) for the five mergers as a function of time. Increasing the mass ratio of the merger systematically lowers the

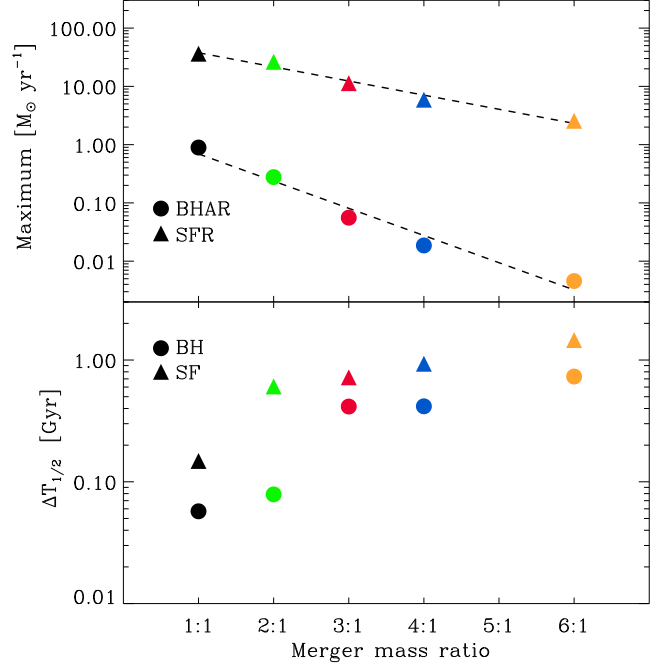


FIG. 9.— The maximum BH accretion and star formation rates and timescales as a function of merger mass ratio. The bottom panel shows the half mass growth time of the BHs (circles) and the stellar mass (triangles) centered on the maximum BH accretion and star formation rates, respectively. The top panel shows the corresponding peak BH accretion (circles) and star formation rates (triangles) during the corresponding half mass growth time  $\Delta T_{1/2}$ . The dashed line is the best resulting fit of Eq. 10 to the peak values.

peak star formation rate and increases the duration of star formation activity after the merger. For the highest mass ratio merger the star formation rate is virtually constant throughout the simulation with only a mild peak during the first passage (see also di Matteo et al. 2007; Bournaud et al. 2007b). A similar evolution is seen in the BH accretion rates, with the BH accretion rates systematically peaking at higher rates with decreasing merger mass ratios. For the higher mass ratio mergers no well defined BH accretion peak is discernable, instead the BH accretion rates stay roughly constant on an elevated level for a prolonged time period compared to the pre-merger BH accretion rates. The evolution of the BH accretion rates are mirrored in the growth of the BH masses, with the final BH mass being systematically lower for increasing mass ratio of the merger. Furthermore, the slope of the  $M_{\text{BH}}$  growth as a function of time becomes shallower with increasing merger mass ratio. There is also a systematic delay in the time of the BH merger with increasing mass ratio, as indicated by the filled circles in Fig. 8. For the lower mass ratio mergers the peak of the BH activity (the filled triangles in Fig. 8) typically occurs shortly after the merging of the BHs, whereas for the higher mass ratio mergers the peak of the BH activity is not directly related to the merging time of the BHs.

In Fig. 9 we study the duration of the BH accretion and star formation activity as a function of merger mass ratio. We define a half-mass growth time  $\Delta T_{1/2}$  during which half of the final BH mass and half of the total stellar mass is formed respectively. In both cases  $\Delta T_{1/2}$  is centered on the peak of the corresponding activity,

the BH accretion on the maximum of the BH accretion rate (the triangles in Fig. 8) and the star formation rate on the peak of the SFR marked with diamonds in Fig. 8. The resulting half-mass timescales are shown in the bottom panel of Fig. 9. The  $\Delta T_{1/2\text{BH}}$  is strongly correlated with the mass ratio of the merger. For 1:1 and 2:1 mergers the growth of the  $M_{\text{BH}}$  is very concentrated in time, with half of the final BH mass growth occurring in less than 100 Myr. For the 3:1 and 4:1 mergers  $\Delta T_{1/2\text{BH}} \sim 0.5$  Gyr, with the 6:1 merger resulting in  $\Delta T_{1/2\text{BH}} \sim 1$  Gyr. In the lower mass ratio mergers a significant fraction of the gas is funnelled to the center during the merger, enabling the BHs to experience rapid Eddington limited growth (Eq. 2). For larger mass ratio mergers the tidally driven non-axisymmetric torques are weaker and a lower fraction of the gas reaches the center resulting in lower BH accretion rates and longer BH half-mass growth timescales.

The corresponding stellar half-mass timescales  $\Delta T_{1/2\text{star}}$  (triangles in the bottom panel Fig. 9) also show a clear correlation with the mass ratio of the merger. In the 1:1 merger half of the final stellar mass is formed in a short major burst lasting about  $\Delta T_{1/2\text{star}} \sim 0.15$  Gyr. This value is comparable to the star formation timescale derived by Cox et al. (2008), who calculated a full width at half maximum of FWHM  $\sim 0.1$  Gyr for the star formation peak of a typical 1:1 merger. For higher mass-ratio mergers the resulting star formation timescales are  $\Delta T_{1/2\text{star}} \sim 0.7 - 1.0$  Gyr, with the highest mass-ratio merger having the longest timescale of  $\Delta T_{1/2\text{star}} \sim 1.5$  Gyr. In these cases it is not straightforward to relate our  $\Delta T_{1/2\text{star}}$  to the burst timescales defined by Cox et al. (2008), as the higher mass ratio mergers have less well defined star formation peaks with the star formation distributed more evenly over time. However, the general trend that increasing the merger mass ratio results in increasingly longer star formation timescales agrees well with the results of Cox et al. (2008).

Finally we plot in the top panel of Fig. 9 the corresponding maximum black hole accretion and star formation rates during their respective half mass growth timescales. By defining the variable  $q$  as the mass ratio between the primary and secondary component we can fit the logarithms of the peak BH accretion and star formation rates with the following linear relation

$$\log \text{Maximum} [\text{M}_{\odot}\text{yr}^{-1}] = a_0 + a_1 \times q, \quad (10)$$

where  $a_0$  and  $a_1$  are the inferred normalization and slope respectively. Both the maximum BH accretion rates and star formation rates are well fitted by Eq. 10 (dotted lines in Fig. 9) resulting in the following best fitting parameters respectively: ( $a_{0,\text{BHAR}} = 0.31, a_{1,\text{BHAR}} = -0.47$ ) ( $a_{0,\text{SFR}} = 1.82, a_{1,\text{SFR}} = -0.24$ ). The ratio of the peak BH accretion rate to the peak star formation rate is thus of the order of  $\dot{M}_{\text{BH,peak}}/\dot{M}_{\text{SF,peak}} \sim 10^{-2}$ . On the other hand, the ratio of the mean BH accretion rate to the mean star formation averaged over the whole simulation is closer to  $\dot{M}_{\text{BH,mean}}/\dot{M}_{\text{SF,mean}} \sim 10^{-3}$ , with this ratio varying systematically between  $\dot{M}_{\text{BH,mean}}/\dot{M}_{\text{SF,mean}} = 2 \cdot 10^{-3}$  (1:1 merger) and  $\dot{M}_{\text{BH,mean}}/\dot{M}_{\text{SF,mean}} = 0.2 \cdot 10^{-3}$  (6:1

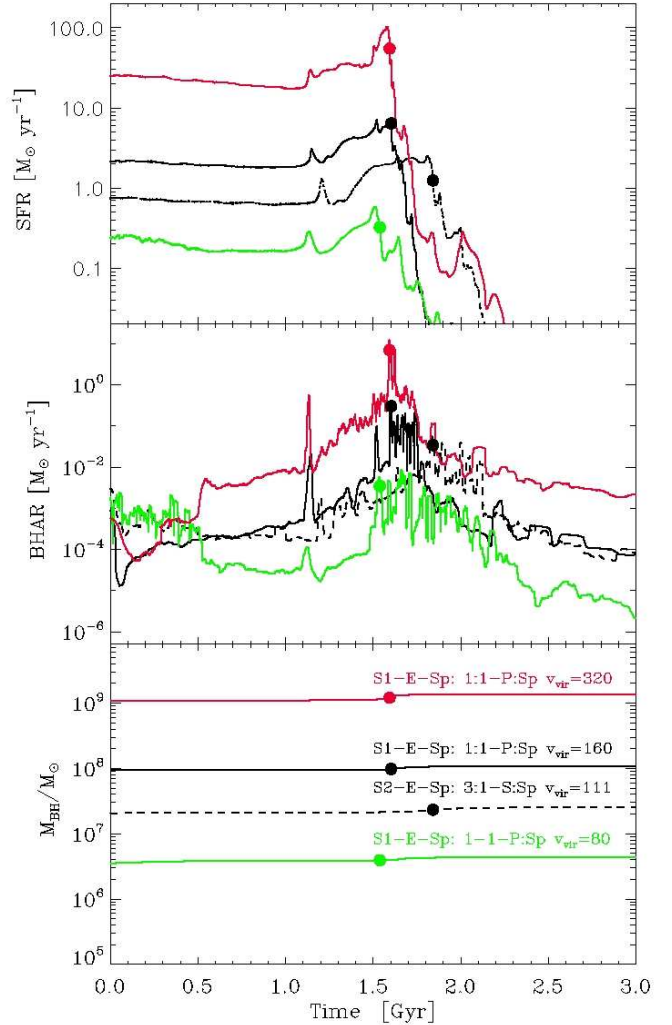


FIG. 10.— The total star formation rate (top), the total black hole accretion rate (middle) and the evolution of the total black hole mass (bottom) as a function of time for four E-Sp mixed mergers. The solid lines show mixed E-Sp mergers of 1:1 merger remnants with primary spiral disks and the dashed line shows a mixed E-Sp merger between a 3:1 merger remnant and a secondary spiral disk. The gas disks have initially  $f_{\text{gas}} = 20\%$  and the virial velocities as indicated in the Figure. The filled circles indicate the time of merging of the BHs.

merger). Interestingly, recent observations of  $z \sim 2$  galaxies by Daddi et al. (2007b,a) also find indications of an universal ratio of  $\dot{M}_{\text{BH}}/\dot{M}_{\text{SF}} \sim 10^{-3}$  and this is also expected from the observed  $M_{\text{BH}} - M_*$  relation. Naturally the normalizations and to some extent the slopes of the derived BH and SFR activity relations are dependent on the initial gas mass fraction and orbital geometry of the system. However, the derived ratios between the BH accretion and SF rates should be valid and we find in our simulations that for any given orbital configuration and initial gas mass fraction the ratio of the peak BH accretion and SF rates is  $\sim 10^{-2}$ , whereas the corresponding mean value is of the order of  $\sim 10^{-3}$ .

#### 4.3. Mixed E-Sp mergers with BHs

We now turn our attention to mixed E-Sp mergers, in which a gas-poor early-type galaxy merges with a gas-rich spiral disk galaxy. To this end we simulated to our

TABLE 6  
 MIXED E-SP MERGERS

Models	Progenitor 1	$v_{\text{vir,prog2}}^a$	Mass ratio	Orbit	$f_{\text{gas,init}}$	$N_{\text{disk,tot}}$	$N_{\text{bulge,tot}}$	$N_{\text{DM,tot}}$	$N_{\text{sim}}$
S1-E-Sp	S1-1:1	50, 80, 160, 320, 500	2:1	G0	0.2	60000	30000	90000	5
S2-E-Sp	S2-3:1	35, 55, 111, 222, 347	4:1	G0	0.2	33334	16666	50000	5
G1-E-Sp	G1-1:1	160	2:1	G7, G10, G13	0.2	60000	30000	90000	3
G2-E-Sp	G2-3:1	111	4:1	G4, G10, G14	0.2	33334	16666	50000	3

<sup>a</sup>All virial velocities in  $\text{kms}^{-1}$

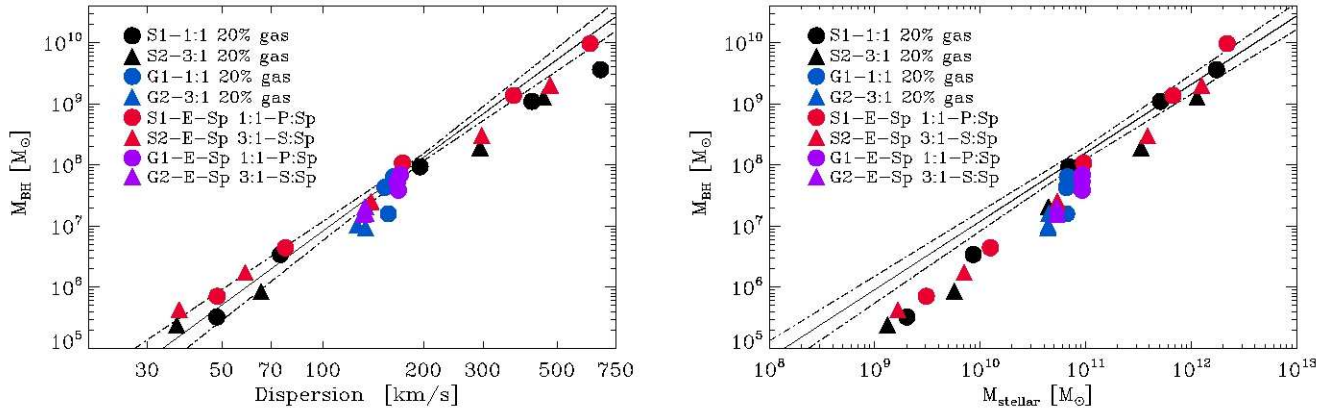


FIG. 11.— The  $M_{\text{BH}} - \sigma$  (left) and  $M_{\text{BH}} - M_*$  (right) relations for our sample of mixed E-Sp mergers. The merger remnants of the original 1:1 and 3:1 mergers are shown by black and blue filled circles and triangles for the S and G merger series, respectively (Table 3). The mixed merging of 1:1 merger remnants with primary spiral disks with  $f_{\text{gas}} = 20\%$  (1:1-P:Sp) are shown with filled red (S1-series) and purple (G1-series) circles. The mixed merging of 3:1 merger remnants with secondary spiral disks with  $f_{\text{gas}} = 20\%$  (3:1-S:Sp) are shown with filled red (S2-series) and purple (G2-series) triangles. The lines show the observed relations with errors by Tremaine et al. (2002) (left panel) and Häring & Rix (2004) (right panel), respectively.

knowledge for the first time a large sample of mixed E-Sp mergers. For early-type progenitors we use the merger remnants of 1:1 and 3:1 mergers discussed in §4.1, whereas the progenitor disk galaxies are setup using the disk models discussed in §3.1. Our mixed merger sample consisted of five 1:1 merger remnants that are merged with the primary disks of the original simulations (S1-E-Sp) and another five runs in which 3:1 merger remnants are merged with the corresponding secondary disks of the original simulations (S2-E-Sp). This sample of ten mixed mergers were run on the same G0 orbit as the original mergers. In addition, we simulated six E-Sp mergers of 1:1 and 3:1 merger remnants with primary and secondary disks respectively (G1-E-Sp and G2-E-Sp) with varying initial orientations and orbital geometries as indicated in Table 6. This results in a total sample of 16 mixed E-Sp mergers. The initial gas fraction was set to 20% in both the original simulations that produced the E-progenitors and in the disk progenitors. The black hole mass of the early-type progenitors is set by the result in the original simulation and is typically  $M_{\text{BH}} \sim 10^6 - 10^9 M_{\odot}$ , whereas the initial seed BH mass of the disk galaxies is always fixed at  $M_{\text{BH}} = 10^5 M_{\odot}$ .

We plot the corresponding total star formation rates (top), the total BH accretion rates (middle) and the evolution of the total BH mass (bottom) in Fig. 10 for a sample of four mixed E-Sp mergers. The three solid lines show mergers between 1:1 merger remnants and primary disks and the dashed line a merger between a 3:1 merger remnant and a secondary disk, with the color scaling indicating the virial velocity of the disk progenitors. The combined star formation rate of the mixed E-Sp mergers

TABLE 7  
 BEST FIT  $M_{\text{BH}} - \sigma$  RELATION FOR E-E AND E-SP MERGERS

Sample	N	$a$	$b$	$\Delta_{\log M_{\text{BH}}}$
Progenitor sample	16	$7.83 \pm 0.04$	$3.53 \pm 0.11$	0.16
E-Sp Mixed sample	16	$8.03 \pm 0.04$	$3.55 \pm 0.12$	0.13
E-E Remerger sample	16	$8.13 \pm 0.05$	$3.41 \pm 0.10$	0.18

is lower than in Sp-Sp (Fig. 5) mergers, due to the lower amount of cold gas available for star formation. The disk progenitor contains  $f_{\text{gas}} = 20\%$  of gas initially, whereas the early-type progenitors typically have an initial gas mass fraction of  $f_{\text{gas}} \sim 5\%$ , with typically only  $\sim 1\%$  of this gas being cold and dense. After the merger of the E-Sp galaxies the star formation rate declines rapidly in all the merger remnants. The black hole accretion rates are somewhat lower than in Sp-Sp mergers, but still relatively high due to the large amount of available gas in the central regions of the merger remnants originating from the disk progenitors. The BH accretion rates show a clear peak, both during the time of the first passage and at the time of final coalescence. We define a BH mass growth factor as  $f_{\text{BH,insitu}} = \Delta M_{\text{BH,insitu}} / M_{\text{BH,final}}$ , which gives the ratio of BH mass growth due to gas accretion during the simulation with respect to the final BH mass. Quantitatively, the fraction of the BH mass that accumulates by gas accretion during the mixed mergers is in the range of  $f_{\text{BH,insitu}} \sim 20 - 50\%$ , with typical mean values of  $f_{\text{BH,insitu}} \sim 30\%$ . Thus in most cases the majority of the final BH mass is still contributed by the massive seed BHs residing in the early-type progenitors.

The  $M_{\text{BH}} - \sigma$  (left panel) and  $M_{\text{BH}} - M_*$  (right panel) relations for our mixed E-Sp merger (red and purple sym-

TABLE 8  
BEST FIT  $M_{\text{BH}} - M_*$  RELATION FOR E-E AND E-SP MERGERS

Sample	N	c	d	$\Delta_{\log M_{\text{BH}}}$
Progenitor sample	16	$7.78 \pm 0.07$	$1.35 \pm 0.05$	0.21
E-Sp Mixed sample	16	$7.83 \pm 0.05$	$1.39 \pm 0.07$	0.16
E-E Remerger sample	16	$7.86 \pm 0.05$	$1.38 \pm 0.04$	0.17

bols) sample together with the E-type progenitor population (black and blue symbols) is plotted in Fig. 11. All the progenitor disk galaxies have initial seed BH masses of  $M_{\text{BH}} = 10^5 M_{\odot}$  with the velocity dispersion  $\sigma$  depending on the bulge mass of the progenitor galaxy. Thus the BHs of the disk galaxies are not initially on the  $M_{\text{BH}} - \sigma$  relation and they are also not plotted in Fig. 11. Using a least-squares fit and Bootstrap technique we derive the best fitting parameters for the  $M_{\text{BH}} - \sigma$  relation of our mixed merger and progenitor samples (see Table 7). For the mixed mergers the normalization parameter  $a$  is 0.2 dex higher than for the Sp-Sp progenitor sample, but 0.1 dex lower than for the E-E mergers. The combined in-situ growth due to gas accretion and merging of the BHs thus result in final BH masses that are very similar to the ones derived in both the Sp-Sp (Fig. 7) and E-E mergers (Fig. 13). The mixed merging of E-Sp galaxies seems to maintain the slope  $b$  of the  $M_{\text{BH}} - \sigma$  relation compared to the progenitor sample and even slightly reduces the dispersion. The mixed mergers primarily increase the final BH mass, with smaller changes in the final velocity dispersion compared to the initial dispersion of the early-type progenitors. Overall the slope and dispersion are lower than the observed Tremaine et al. (2002) values of  $b = 4.02 \pm 0.32$ ,  $\Delta_{\log M_{\text{BH}}} = 0.25 - 0.3$ . This is primarily due to the fact that all of the original mergers and disk progenitors had initial gas mass fractions of 20%. Including mixed mergers of merger remnants and disks with higher initial gas mass fractions would increase the normalization, slope and scatter in the derived  $M_{\text{BH}} - \sigma$  relation (see Table 4). The mixed mergers undergo a similar phase of strong self-regulated BH growth as the Sp-Sp mergers, allowing the BH feedback to regulate the final BH mass in agreement of the  $M_{\text{BH}} - \sigma$  relation. Thus we conclude that the  $M_{\text{BH}} - \sigma$  relation should remain relatively stable even after several generations of mixed E-Sp mergers.

Finally, we also perform a least-squares fit to the  $M_{\text{BH}} - M_*$  (Eq. 9) relation for our mixed E-Sp sample with the best fit parameters listed in Table 8. The mixed merging of an E-Sp galaxy population effectively maintains the original  $M_{\text{BH}} - M_*$  relation of the progenitor sample, even slightly reducing the intrinsic dispersion in the relation. The self-regulated stellar and BH feedback models regulate the star formation process and BH mass growth in mixed mergers similarly to Sp-Sp mergers thus ensuring that the derived original  $M_{\text{BH}} - M_*$  relation is maintained. We thus conclude that even repeated generations of mixed E-Sp mixed mergers should not greatly affect the observed  $M_{\text{BH}} - M_*$  relation.

#### 4.4. E-E remergers with BHs

Finally, we studied E-E mergers including BH feedback by remerging a sample of our merger remnants produced by the 3:1 and 1:1 mergers discussed in §4.1. We set up and ran five equal-mass remergers of our S1-1:1 (Table

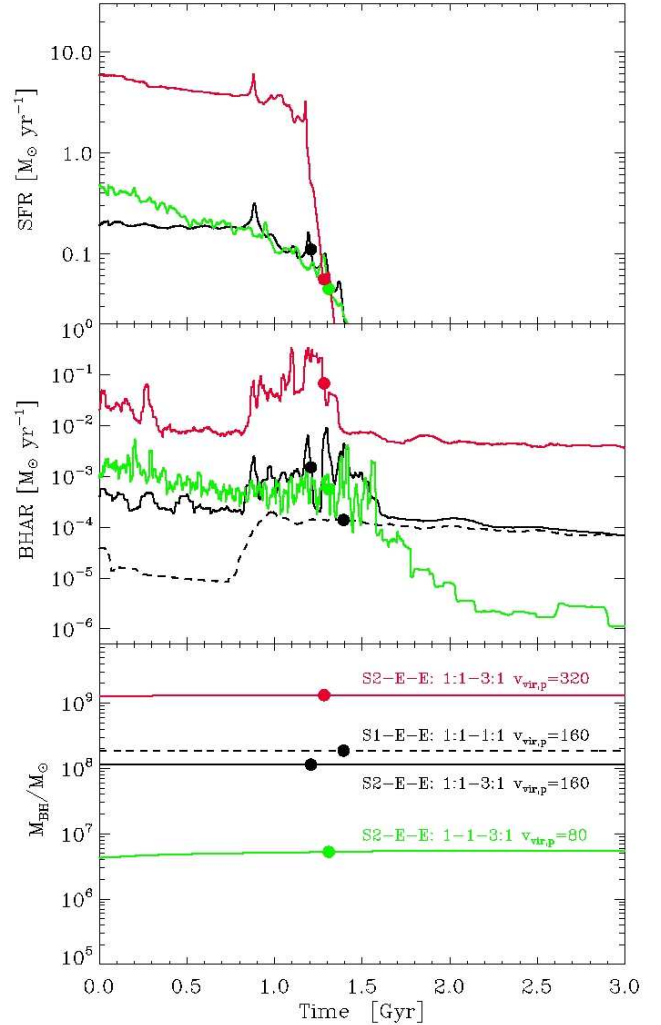


FIG. 12.— The total star formation rate (top), the black hole accretion rate (middle) and the evolution of the total black hole mass (bottom) as a function of time for four E-E remergers. The solid lines show remergers between 1:1 and 3:1 merger remnants and the dashed line shows a E-E remerger between two 1:1 merger remnants. The virial velocities of the primary galaxies in the original simulations are as indicated in the Figure. The filled circles indicate the time of merging of the BHs.

3) merger remnants (S1-E-E), with the initial progenitor disks of the original simulations having virial velocities in the range  $v_{\text{vir}} = 50 - 500 \text{ km s}^{-1}$ . In addition, we remerged five of our 1:1 merger remnants with the corresponding set of 3:1 merger remnants (S2-E-E), resulting in a mass ratio of 3:2 (see Table 9). All of the mergers were run on identical orbits to the original mergers and the initial gas fraction of the progenitors for the original simulations was fixed at 20%. In addition to the ten S-series remergers that were run on the G0 orbit, we simulated three E-E mergers of 1:1 merger remnants (G1-E-E) and three E-E mergers of 3:1 merger remnants (G2-E-E) with varying initial orientations and orbital geometries as indicated in Table 9, thus resulting in a total sample of 16 E-E remergers.

In Fig. 12 we plot the star formation rate (top), the BH accretion rate (middle) and the evolution of the BH mass (bottom) for three 1:1-3:1 E-E remergers (solid lines) and one 1:1-1:1 E-E remerger (dashed line). Here the color-

TABLE 9  
 E-E REMERGERS

Models	Progenitor 1	Progenitor 2	Mass ratio	Orbit	$f_{\text{gas,init}}$	$N_{\text{disk,tot}}$	$N_{\text{bulge,tot}}$	$N_{\text{DM,tot}}$	$N_{\text{sim}}$
S1-E-E	S1-1:1	S1-1:1	1:1	G0	0.2	80000	40000	120000	5
S2-E-E	S1-1:1	S2-3:1	3:2	G0	0.2	66667	33333	100000	5
G1-E-E	G1-1:1	G1-1:1	1:1	G7, G10, G13	0.2	80000	40000	120000	3
G2-E-E	G2-3:1	G2-3:1	1:1	G4, G10, G14	0.2	26666	53334	80000	3

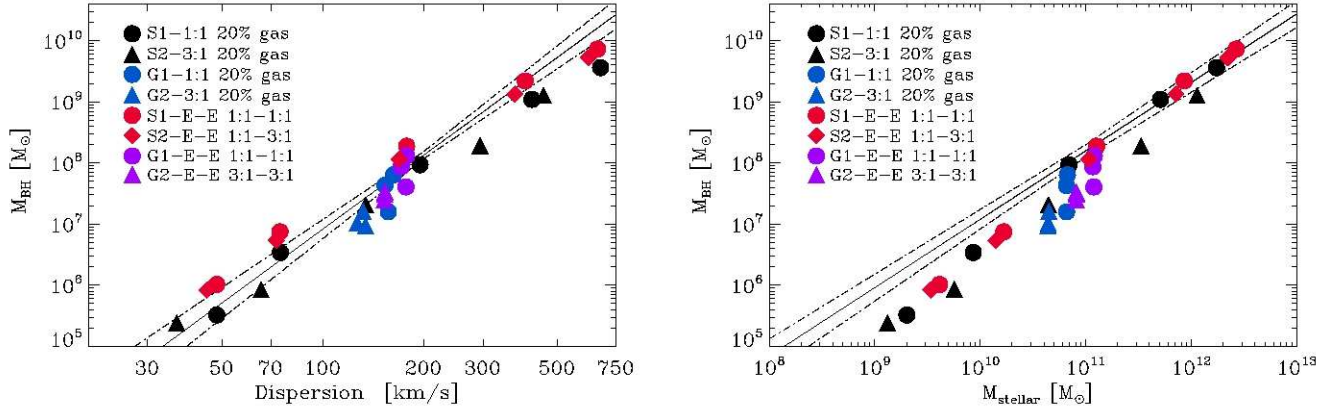


FIG. 13.— The  $M_{\text{BH}} - \sigma$  (left) and  $M_{\text{BH}} - M_*$  (right) relations for our sample of E-E remergers. The merger remnants of the original 1:1 and 3:1 mergers are shown by black and blue filled circles and triangles for the S and G merger series, respectively (Table 3). The remerging of 1:1-1:1 merger remnants are shown with filled red (S1-series) and purple (G1-series) circles, the remerging of 1:1-3:1 merger remnants (S2-series) are shown with red diamond symbols and finally the remerging of 3:1-3:1 remnants (G2-series) by purple triangles. The lines show the observed relations with errors by Tremaine et al. (2002) (left panel) and Häring & Rix (2004) (right panel), respectively.

ing indicates the virial velocities of the primary galaxies in the original simulations,  $v_{\text{vir,p}} = 80 \text{ km s}^{-1}$  (green),  $v_{\text{vir,p}} = 160 \text{ km s}^{-1}$  (black) and  $v_{\text{vir,p}} = 320 \text{ km s}^{-1}$  (red). The initial star formation rates are generally very low due to the low gas fractions of  $f_{\text{gas}} \sim 1 - 5\%$  and  $f_{\text{gas}} \sim 5 - 10\%$  for the 1:1 and 3:1 merger remnant E-progenitors, respectively. The initial gas fraction directly depends on the strength of the initial interaction that gave rise to the merger remnants used as progenitors for the E-E remergers. Increasing the masses of the progenitors and using more direct planar orbits (G0) produces more violent initial encounters, thus decreasing  $f_{\text{gas}}$ . In addition, most of the gas is hot with low densities and the fraction of cold star-forming gas is typically below  $\lesssim 1\%$  of the total gas mass. As can be seen in Fig. 12 the star formation is very effectively terminated shortly after the merging of the E-E progenitors on comparable timescales to 1:1 Sp-Sp mergers and thus more efficiently than in 3:1 Sp-Sp and mixed E-Sp mergers. For the 1:1-1:1 E-E remerger the star formation rate is zero throughout the simulation as the star formation was already completely terminated in the original 1:1 merger that served as a progenitor galaxy for the E-E merger (see Figs. 5 and 8).

The black hole accretion rates strongly correlate with the available amount of gas in the central regions and are thus typically one to two orders of magnitude lower for dry E-E mergers compared to the mixed E-Sp and Sp-Sp mergers. This is also reflected in the total BH mass growth plots (Fig. 12) that remain virtually flat throughout the simulations. The growth of the final BH mass is primarily due to the merging of the BHs with the in-situ growth of the BH mass through gas accretion being relatively low. The exact fraction of BH mass

grown in-situ ( $f_{\text{BH,insitu}}$ ) due to gas accretion during the simulation with respect to the final BH mass, depends on the amount of available gas initially. For remerging of 1:1 merger remnants this fraction is typically very low at  $f_{\text{BH,insitu}} < 1\%$ , whereas for the remerging of 1:1-3:1 merger remnants the fraction is higher at  $f_{\text{BH,insitu}} \sim 10\%$ , with the highest fraction of  $f_{\text{BH,insitu}} \sim 20\%$  produced for remerging of 3:1-3:1 merger remnants, as expected. There is relatively large scatter in the  $f_{\text{BH,insitu}}$  fraction as a function of the orbital configuration and the initial masses of the progenitor galaxies primarily set by the corresponding scatter in the initial gas mass fractions of the progenitor galaxies. All the fractions above are estimates for only first generation remergers, with the  $f_{\text{BH,insitu}}$  ratio rapidly decreasing with increasing generations of remergers. The same is true for the star formation, E-E remerging effectively quenches the star formation (Fig. 12) and already a second generation of dry merging is expected to show very weak, if any, signatures of residual star formation.

In Fig. 13 we plot the  $M_{\text{BH}} - \sigma$  (left panel) and the  $M_{\text{BH}} - M_*$  (right panel) relations for our E-E remerger (red and purple symbols) sample together with the progenitor population (black and blue symbols). The best fitted  $M_{\text{BH}} - \sigma$  parameters together with the  $1\sigma$  uncertainties for our E-E remerger sample are listed in Table 7. The normalization parameter  $a$  is 0.3 dex higher for the E-E remerger sample compared to the progenitor sample and 0.1 dex higher compared to the mixed E-Sp sample. However the slope  $b$  is marginally shallower compared to both the progenitor and mixed merger samples. The E-E remerging of the merger remnants increases the final BH mass, but leaves the velocity dispersion more or less unchanged, resulting in an increase of  $a$ . The relative

increase in  $M_{\text{BH}}$  is slightly larger for low-mass systems compared to higher-mass systems, resulting in a slightly lower slope  $b$ . This is especially true for the remergers on the G0 orbit, whereas remergers on other orbits (the purple G-series in Fig. 13) also increase slightly the velocity dispersion of the resulting merger remnants (see also Robertson et al. 2006a). The overall lower value of the slope  $b$  is again due to the fact that only E-E mergers of progenitors with initial gas fractions of  $f_{\text{gas}} = 20\%$  in the original simulations were included in constructing the E-E sample. We thus conclude that dry E-E remerging typically increases the normalization parameter  $a$  and lowers the slope  $b$  slightly, but a single generation of dry remerging is not able to destroy the  $M_{\text{BH}} - \sigma$  relation initially generated by gas-rich mergers (see also Robertson et al. 2006a). E-E remerging also increases slightly the dispersion in the fitted relation, but the variation in the initial gas fraction still remains the dominant source of scatter. Unlike Sp-Sp and mixed E-Sp mergers the gas-poor E-E mergers only experience a weak self-regulatory BH growth phase, with this phase missing altogether for the gas-poorest E-E mergers. This lack of the self-regulating feedback phase can thus explain some of the larger scatter in the final E-E remerger  $M_{\text{BH}} - \sigma$  relation.

We also perform a least-squares fit to the  $M_{\text{BH}} - M_*$  (Eq. 9) relation for both the E-E remerger sample and the progenitor sample with the best fit parameters, parameter errors and dispersions listed in Table 8. Dry E-E remerging effectively maintains the normalization coefficient ( $c$ ) and slope ( $d$ ) of the progenitor sample, with a very minor increase of both parameters that lie within the  $1\sigma$  uncertainties of the corresponding progenitor parameters. Furthermore dry remerging roughly maintains the dispersion derived for the progenitor population. This is expected since the in-situ growth from gas of both the BH and stellar mass are very low during the simulation. For the limiting case of no available gas and no in-situ growth of the BH and stellar mass, the original  $M_{\text{BH}} - M_*$  relation would be perfectly conserved. Thus we expect that increasing generations of E-E mergers would not substantially increase the scatter in the observed  $M_{\text{BH}} - M_*$  relation. The discrepancy between the derived  $M_{\text{BH}} - M_*$  parameters for the E-E remergers and the observed parameters would be remedied by remerging merger remnants with higher initial gas mass fractions (increases  $c$ ) and by employing more effective stellar feedback models (lowers  $d$ ) as was already discussed in §4.1.

## 5. SUMMARY AND DISCUSSION

In this paper, we calculate the  $M_{\text{BH}} - \sigma$  and  $M_{\text{BH}} - M_*$  relations produced by merging equal- and unequal-mass disk progenitors, mixed disk-elliptical progenitors and elliptical-elliptical progenitors. Our simulation sample consists of 18 equal-mass, 18 unequal-mass disk mergers, 16 mixed E-Sp mergers and 16 dry E-E mergers producing a total merger sample of 68 mergers. The simulations include radiative cooling, star formation and black holes with their associated feedback processes as described in Springel et al. (2005b). All simulations reproduce the observed  $M_{\text{BH}} - \sigma$  relation, with the dominant source of scatter arising from variations in the initial gas mass fractions of the disk galaxies. The normalization of the

observed  $M_{\text{BH}} - M_*$  relation is also well fitted in our simulation sample, but with the resulting slope being slightly steeper compared to the observed slope. However, we do have to caution that the actual bulge/disk fraction for the merger remnants is not known. Very gas-rich disk mergers can result in merger remnants with disk-like morphologies (Springel & Hernquist 2005) and disk merger remnants cover a large range of bulge-to-disk ratios when careful disk-bulge decompositions are applied (Naab & Trujillo 2006). For a consistent comparison with observations such a photometric decomposition needs to be applied, in particular for higher mass ratio disk mergers (Naab et al. in prep).

The discrepancy between the observed and simulated slope of the  $M_{\text{BH}} - M_*$  relation could also be resolved by employing a more aggressive supernova-driven wind feedback that would primarily lower the stellar mass in the lower-mass stellar systems. Finally, self-consistent cosmological simulations (Sijacki et al. 2007; Di Matteo et al. 2007) employing supernova-driven wind and BH feedback also reproduce the observed normalizations and slopes of the  $M_{\text{BH}} - \sigma$  and  $M_{\text{BH}} - M_*$  relations. The remarkable robustness of the simulated  $M_{\text{BH}} - \sigma$  and  $M_{\text{BH}} - M_*$  relations for an extremely wide range of initial galaxy properties implies that the Springel et al. (2005b) effective BH feedback model self-regulates the mass growth of the BHs in accordance with the observed relations for a very wide range of merger progenitors. The key requirements for the BH feedback model are as follows:

1. The model needs to allow for large-scale gas flows to the central regions of the galaxy in order to feed the central BH. Mechanisms include the central transport of gas due to tidal torques produced by galaxy mergers, and secular effects, such as viscous transport and disk instabilities. The runs with BH feedback in disk galaxies performed in §3.3 showed that in general the galaxies do not evolve in isolation onto the  $M_{\text{BH}} - \sigma$  and  $M_{\text{BH}} - M_*$  relations, with the majority of galaxies requiring additional gas flows to their central regions in order to fulfill the observed relations.

2. A certain fraction of the gas in the central region needs to be accreted onto the BH. In the simplest model one can either assume a constant accretion fraction or a mass-dependent accretion that scales with the circular velocity of the surrounding dark matter halo (Haehnelt & Kauffmann 2000). Dasyra et al. (2006c) also showed (their Fig. 9) that their merger remnants would fall on the observed  $M_{\text{BH}} - \sigma$  relation after the first encounter and further stay on the relation if a fixed fraction of  $\sim 1\%$  of the central gas reservoir was accreted onto the BH. In the Bondi-Hoyle-Lyttleton parameterization used in the Springel et al. (2005b) model the accretion rate depends in a more physical way on the BH mass and the surrounding environment. The critical parameter is the accretion efficiency parameter  $\alpha$  that needs to be large enough to allow BHs in a gas-rich environment to reach Eddington-limited accretion rates (Springel et al. 2005b). Furthermore a large value for  $\alpha$  can also be seen as an empirical correction factor that corrects for the fact that low-resolution simulations are unable to resolve the high-density gas expected at the location of the BH (see §3.2). As was shown in Figs. 8

and 9 the bulk of the BH mass growth for high mass ratio disk mergers takes place during a short time interval centered on the accretion peak during which time the BHs accrete at or very close to their Eddington limits. Too low accretion efficiencies  $\alpha$  result in very low accretion rates stifling the growth of the BH and resulting in too low final BH masses for a given  $\sigma$  and  $M_*$  (see Fig 2).

3. The efficiency of the energy feedback parameters  $\epsilon_r$  and  $\epsilon_f$  need to be set correctly as they determine the normalization of the derived  $M_{\text{BH}} - \sigma$  and  $M_{\text{BH}} - M_*$  relations. Too low energy efficiency parameters allow prolonged BH accretion resulting in too large final BH masses, whereas too high energy efficiencies produce too aggressive BH feedback, limiting too strongly the mass growth of the BH. Thus the correct choice of  $\epsilon_r$  and  $\epsilon_f$  is necessary in producing the observed normalization of the relations (Di Matteo et al. 2005). On the other hand, the slope and produced scatter of the relations is not adjustable by free parameters and is a product of the self-regulation of the feedback model (Sijacki et al. 2007). Once fixed using equal-mass disk mergers neither the accretion nor the energy efficiency parameters need to be modified when running our wide range of initial progenitor models with varying gas fractions and initial morphologies. This indicates that the chosen values of  $\alpha = 100$ ,  $\epsilon_r = 0.1$  and  $\epsilon_f = 0.05$  reproduce robustly the physics underlying the BH feedback model given the physical limitations inherent in the model.

4. The model conserves momentum during the merging of the BHs, which can produce a relatively large 'kick' for the final BH. This is especially true for unequal-mass mergers where the mass ratio of the merging BHs is typically relatively large. This can displace the final BH from the central gas disk and some mechanism is needed to ensure that the BH after the merger can continue accreting gas from the surrounding medium. We have shown in this paper that this can be achieved by repositioning the BH on the minimum of the local gravitational potential at every timestep. This repositioning ensures that the final BH quickly resettles in the central gas disk after the merging of the BHs. Typically the BH reaches its peak accretion rate shortly after the merging of the BHs (see Fig. 8) and this short phase of Eddington limited mass growth is typically required in order for the final BH to reach the observed  $M_{\text{BH}} - \sigma$  and  $M_{\text{BH}} - M_*$  relations.

In addition we study the termination of star formation in merger simulations including BH feedback. Confirming earlier studies (Springel et al. 2005a) we show that equal-mass disk mergers with BHs are very efficient in terminating star formation. However, this termination of star formation is significantly less efficient in unequal-mass disk mergers, with the timescale for star formation termination systematically increasing with increasing progenitor mass ratios. Similarly, a systematic increase is seen in the mass growth timescales of the BHs, with half of the final BH growth mass occurring in 0.1 Gyr (1:1) and 1 Gyr (6:1) mergers, respectively. For mass-ratios of 3:1 and higher mergers with BH feedback are unable to completely quench the star formation, with the merger remnants showing star formation rates roughly on the pre-merger level even 1 Gyr after completion of the merger. In addition mixed E-Sp and dry E-E mergers are very efficient in terminating residual star formation. E-E mergers even to such an extent that already

a second generation of dry merging is expected to show very weak, if any, signatures of residual star formation.

We thus conclude that the combined effect of large-scale gas flows to the central regions together with a self-regulated model of BH feedback thus robustly reproduces the observed  $M_{\text{BH}} - \sigma$  and  $M_{\text{BH}} - M_*$  relations. However, in addition it is important to study the detailed properties of merger remnants including BH feedback. The influence of the formation of a supermassive BH on the properties of merger remnants still has to be investigated in detail. It has been shown that the stellar orbits, e.g. the relative population of box and tube orbits, in merger remnants are affected by the amount of gas driven to the center (Barnes & Hernquist 1996; Jesseit et al. 2005, 2007). Here, even relatively small amounts of gas ( $\sim 5\%$ ) can influence higher order photometric and kinematical properties of the remnants as a whole (Naab et al. 2006a). As efficient feedback from black holes (and from stars Khochfar & Silk 2006a,b) reduces the central gas content in first generation disk merger remnants, future mergers will be less dissipative and favor the formation of triaxial stellar systems dominated by box orbits (Jesseit et al. 2005; Naab et al. 2006a). However, stars on box orbits can be affected by the central black holes on much longer time scales in isolated galaxies (Milosavljević & Merritt 2001). It is difficult to compare the intrinsic shape, anisotropy and orbital content of observed ellipticals to simulated remnants. A first step in this direction has been taken by Thomas et al. (2007) who applied Schwarzschild modeling to simulated collisionless merger remnants. Further investigations (see e.g. Cox et al. 2006) will show in how far supermassive BHs leave signatures on observable properties, e.g. the central 2D kinematics (Jesseit et al. 2007) or light profiles (Naab & Trujillo 2006). In Burkert et al. (2007) we studied the intrinsic anisotropy  $\delta$  and flattening  $\epsilon$  of simulated merger remnants with and without BH feedback. Here, an equally good fit to ellipticals observed by SAURON (Emsellem et al. 2004; Cappellari et al. 2006) was found in both models that included BH feedback and models without BHs. However, binary disk mergers and their descendants were shown to preferentially form anisotropic systems with relatively high ellipticities, not consistent with observed isotropic and round ellipticals. This is kinematical evidence that some ellipticals cannot have formed by mergers of disks in the first place. There is additional evidence for alternative formation scenarios from stellar population considerations (Naab & Ostriker 2007) as well as direct cosmological simulations (Naab et al. 2007).

AGNs are emerging as an important ingredient in our current galaxy formation models. Research on understanding the observed  $M_{\text{BH}} - \sigma$  and  $M_{\text{BH}} - M_*$  relations using numerical techniques should therefore be a useful step in our quest to formulate a more complete theory of galaxy formation.

We would like to thank R. Jesseit, J. Sommer-Larsen, V. Springel and M. Wetzstein for stimulating discussions and helpful comments on the manuscript. The numerical simulations were performed on the local SGI-Altix 3700 Bx2, which was partly funded by the Cluster of Excellence: "Origin and Structure of the Universe".

## REFERENCES

- Adams, F. C., Graff, D. S., & Richstone, D. O. 2001, *ApJ*, 551, L31
- Arad, I. & Johansson, P. H. 2005, *MNRAS*, 362, 252
- Barger, A. J., Cowie, L. L., Mushotzky, R. F., Yang, Y., Wang, W.-H., Steffen, A. T., & Capak, P. 2005, *AJ*, 129, 578
- Barnes, J. E. 1998, in *Saas-Fee Advanced Course 26: Galaxies: Interactions and Induced Star Formation*, ed. R. C. Kennicutt, Jr., F. Schweizer, J. E. Barnes, D. Friedli, L. Martinet, & D. Pfenniger, 275–+
- Barnes, J. E. 2002, *MNRAS*, 333, 481
- Barnes, J. E. & Hernquist, L. 1996, *ApJ*, 471, 115
- Bate, M. R. & Burkert, A. 1997, *MNRAS*, 288, 1060
- Bell, E. F., Naab, T., McIntosh, D. H., Somerville, R. S., Caldwell, J. A. R., Barden, M., Wolf, C., Rix, H.-W., Beckwith, S. V., Borch, A., Häussler, B., Heymans, C., Jahnke, K., Jogee, S., Kuposov, S., Meisenheimer, K., Peng, C. Y., Sanchez, S. F., & Wisotzki, L. 2006, *ApJ*, 640, 241
- Bondi, H. 1952, *MNRAS*, 112, 195
- Bondi, H. & Hoyle, F. 1944, *MNRAS*, 104, 273
- Bournaud, F., Elmegreen, B. G., & Elmegreen, D. M. 2007a, *ApJ*, 670, 237
- Bournaud, F., Jog, C. J., & Combes, F. 2005, *A&A*, 437, 69
- . 2007b, *A&A*, 476, 1179
- Bower, R. G., Benson, A. J., Malbon, R., Helly, J. C., Frenk, C. S., Baugh, C. M., Cole, S., & Lacey, C. G. 2006, *MNRAS*, 370, 645
- Boylan-Kolchin, M., Ma, C.-P., & Quataert, E. 2005, *MNRAS*, 362, 184
- Bullock, J. S., Kolatt, T. S., Sigad, Y., Somerville, R. S., Kravtsov, A. V., Klypin, A. A., Primack, J. R., & Dekel, A. 2001, *MNRAS*, 321, 559
- Burkert, A. & Naab, T. 2005, *MNRAS*, 363, 597
- Burkert, A., Naab, T., & Johansson, P. H. 2007, *ArXiv e-prints*, 710
- Burkert, A. & Silk, J. 2001, *ApJ*, 554, L151
- Canalizo, G. & Stockton, A. 2001, *ApJ*, 555, 719
- Cappellari, M., Bacon, R., Bureau, M., Damen, M. C., Davies, R. L., de Zeeuw, P. T., Emsellem, E., Falcón-Barroso, J., Krajnović, D., Kuntschner, H., McDermid, R. M., Peletier, R. F., Sarzi, M., van den Bosch, R. C. E., & van de Ven, G. 2006, *MNRAS*, 366, 1126
- Cattaneo, A., Haehnelt, M. G., & Rees, M. J. 1999, *MNRAS*, 308, 77
- Ciotti, L. & Ostriker, J. P. 1997, *ApJ*, 487, L105+
- . 2007, *ApJ*, 665, 1038
- Ciotti, L. & van Albada, T. S. 2001, *ApJ*, 552, L13
- Cox, T. J., Dutta, S. N., Di Matteo, T., Hernquist, L., Hopkins, P. F., Robertson, B., & Springel, V. 2006, *ApJ*, 650, 791
- Cox, T. J., Jonsson, P., Somerville, R. S., Primack, J. R., & Dekel, A. 2008, *MNRAS*, 33
- Cretton, N., Naab, T., Rix, H.-W., & Burkert, A. 2001, *ApJ*, 554, 291
- Croton, D. J., Springel, V., White, S. D. M., De Lucia, G., Frenk, C. S., Gao, L., Jenkins, A., Kauffmann, G., Navarro, J. F., & Yoshida, N. 2006, *MNRAS*, 365, 11
- Daddi, E., Alexander, D. M., Dickinson, M., Gilli, R., Renzini, A., Elbaz, D., Cimatti, A., Chary, R., Frayer, D., Bauer, F. E., Brandt, W. N., Giavalisco, M., Grogan, N. A., Huynh, M., Kurk, J., Mignoli, M., Morrison, G., Pope, A., & Ravindranath, S. 2007a, *ApJ*, 670, 173
- Daddi, E., Dickinson, M., Morrison, G., Chary, R., Cimatti, A., Elbaz, D., Frayer, D., Renzini, A., Pope, A., Alexander, D. M., Bauer, F. E., Giavalisco, M., Huynh, M., Kurk, J., & Mignoli, M. 2007b, *ApJ*, 670, 156
- Dasyra, K. M., Tacconi, L. J., Davies, R. I., Genzel, R., Lutz, D., Naab, T., Burkert, A., Veilleux, S., & Sanders, D. B. 2006a, *ApJ*, 638, 745
- Dasyra, K. M., Tacconi, L. J., Davies, R. I., Genzel, R., Lutz, D., Naab, T., Sanders, D. B., Veilleux, S., & Baker, A. J. 2006b, *New Astronomy Review*, 50, 720
- Dasyra, K. M., Tacconi, L. J., Davies, R. I., Naab, T., Genzel, R., Lutz, D., Sturm, E., Baker, A. J., Veilleux, S., Sanders, D. B., & Burkert, A. 2006c, *ApJ*, 651, 835
- Dehnen, W. 2001, *MNRAS*, 324, 273
- di Matteo, P., Combes, F., Melchior, A.-L., & Semelin, B. 2007, *A&A*, 468, 61
- Di Matteo, T., Colberg, J., Springel, V., Hernquist, L., & Sijacki, D. 2007, *ArXiv e-prints*, 705
- Di Matteo, T., Springel, V., & Hernquist, L. 2005, *Nature*, 433, 604
- Efstathiou, G. 2000, *MNRAS*, 317, 697
- Emsellem, E., Cappellari, M., Peletier, R. F., McDermid, R. M., Bacon, R., Bureau, M., Copin, Y., Davies, R. L., Krajnović, D., Kuntschner, H., Miller, B. W., & de Zeeuw, P. T. 2004, *MNRAS*, 352, 721
- Escala, A., Larson, R. B., Coppi, P. S., & Mardones, D. 2004, *ApJ*, 607, 765
- Fabian, A. C. 1999, *MNRAS*, 308, L39
- Ferrarese, L. & Merritt, D. 2000, *ApJ*, 539, L9
- Flanagan, É. É. & Hughes, S. A. 1998, *Phys. Rev. D*, 57, 4535
- Gebhardt, K., Bender, R., Bower, G., Dressler, A., Faber, S. M., Filippenko, A. V., Green, R., Grillmair, C., Ho, L. C., Kormendy, J., Lauer, T. R., Magorrian, J., Pinkney, J., Richstone, D., & Tremaine, S. 2000, *ApJ*, 539, L13
- Genzel, R., Lutz, D., Sturm, E., Egami, E., Kunze, D., Moorwood, A. F. M., Rigopoulou, D., Spoon, H. W. W., Sternberg, A., Tacconi-Garman, L. E., Tacconi, L., & Thatte, N. 1998, *ApJ*, 498, 579
- Genzel, R., Tacconi, L. J., Rigopoulou, D., Lutz, D., & Tecza, M. 2001, *ApJ*, 563, 527
- Granato, G. L., De Zotti, G., Silva, L., Bressan, A., & Danese, L. 2004, *ApJ*, 600, 580
- Haardt, F. & Madau, P. 1996, *ApJ*, 461, 20
- Haehnelt, M. G. & Kauffmann, G. 2000, *MNRAS*, 318, L35
- Häring, N. & Rix, H.-W. 2004, *ApJ*, 604, L89
- Hernquist, L. 1989, *Nature*, 340, 687
- . 1990, *ApJ*, 356, 359
- Hibbard, J. E. & Yun, M. S. 1999, *ApJ*, 522, L93
- Hopkins, P. F., Cox, T. J., Keres, D., & Hernquist, L. 2007a, *ArXiv e-prints*, 706
- Hopkins, P. F., Hernquist, L., Cox, T. J., Di Matteo, T., Martini, P., Robertson, B., & Springel, V. 2005, *ApJ*, 630, 705
- Hopkins, P. F., Hernquist, L., Cox, T. J., Di Matteo, T., Robertson, B., & Springel, V. 2006, *ApJS*, 163, 1
- Hopkins, P. F., Hernquist, L., Cox, T. J., & Keres, D. 2007b, *ArXiv e-prints*, 706
- Houck, J. R., Soifer, B. T., Weedman, D., Higdon, S. J. U., Higdon, J. L., Herter, T., Brown, M. J. I., Dey, A., Jannuzi, B. T., Le Floc'h, E., Rieke, M., Armus, L., Charmandaris, V., Brandl, B. R., & Teplitz, H. I. 2005, *ApJ*, 622, L105
- Hoyle, F. & Lyttleton, R. A. 1939, in *Proceedings of the Cambridge Philosophical Society*, Vol. 34, *Proceedings of the Cambridge Philosophical Society*, 405–+
- Hughes, S. A. 2002, *MNRAS*, 331, 805
- Jesseit, R., Naab, T., & Burkert, A. 2005, *MNRAS*, 360, 1185
- Jesseit, R., Naab, T., Peletier, R. F., & Burkert, A. 2007, *MNRAS*, 376, 997
- Johansson, P. H. & Efstathiou, G. 2006, *MNRAS*, 371, 1519
- Johansson, P. H., Väisänen, P., & Vaccari, M. 2004, *A&A*, 427, 795
- Katz, N., Weinberg, D. H., & Hernquist, L. 1996, *ApJS*, 105, 19
- Kauffmann, G. & Haehnelt, M. 2000, *MNRAS*, 311, 576
- Kazantzidis, S., Mayer, L., Colpi, M., Madau, P., Debattista, V. P., Wadsley, J., Stadel, J., Quinn, T., & Moore, B. 2005, *ApJ*, 623, L67
- Kennicutt, Jr., R. C. 1998, *ARA&A*, 36, 189
- Khalatyan, A., Cattaneo, A., Schramm, M., Gottloeber, S., Steinmetz, M., & Wisotzki, L. 2007, *ArXiv e-prints*, 712
- Khochfar, S. & Burkert, A. 2001, *ApJ*, 561, 517
- . 2003, *ApJ*, 597, L117
- . 2005, *MNRAS*, 359, 1379
- . 2006, *A&A*, 445, 403
- Khochfar, S. & Silk, J. 2006a, *ApJ*, 648, L21
- . 2006b, *MNRAS*, 370, 902
- Kormendy, J. & Richstone, D. 1995, *ARA&A*, 33, 581
- Levine, R., Gnedin, N. Y., Hamilton, A. J. S., & Kravtsov, A. V. 2007, *ArXiv e-prints*, 711
- Lynden-Bell, D. 1967, *MNRAS*, 136, 101
- Madau, P. & Quataert, E. 2004, *ApJ*, 606, L17

- Magorrian, J., Tremaine, S., Richstone, D., Bender, R., Bower, G., Dressler, A., Faber, S. M., Gebhardt, K., Green, R., Grillmair, C., Kormendy, J., & Lauer, T. 1998, *AJ*, 115, 2285
- Makino, J. & Funato, Y. 2004, *ApJ*, 602, 93
- Marconi, A. & Hunt, L. K. 2003, *ApJ*, 589, L21
- Mayer, L., Kazantzidis, S., Madau, P., Colpi, M., Quinn, T., & Wadsley, J. 2007, *Science*, 316, 1874
- McKee, C. F. & Ostriker, J. P. 1977, *ApJ*, 218, 148
- McLure, R. J., Kukula, M. J., Dunlop, J. S., Baum, S. A., O’Dea, C. P., & Hughes, D. H. 1999, *MNRAS*, 308, 377
- Merritt, D. & Milosavljević, M. 2005, *Living Reviews in Relativity*, 8, 8
- Merritt, D., Milosavljević, M., Favata, M., Hughes, S. A., & Holz, D. E. 2004, *ApJ*, 607, L9
- Milosavljević, M. & Merritt, D. 2001, *ApJ*, 563, 34
- Mo, H. J., Mao, S., & White, S. D. M. 1998, *MNRAS*, 295, 319
- Monaghan, J. J. 1992, *ARA&A*, 30, 543
- Murray, N., Quataert, E., & Thompson, T. A. 2005, *ApJ*, 618, 569
- Naab, T. & Burkert, A. 2003, *ApJ*, 597, 893
- Naab, T., Burkert, A., & Hernquist, L. 1999, *ApJ*, 523, L133
- Naab, T., Jesseit, R., & Burkert, A. 2006a, *MNRAS*, 372, 839
- Naab, T., Johansson, P. H., Ostriker, J. P., & Efstathiou, G. 2007, *ApJ*, 658, 710
- Naab, T., Khochfar, S., & Burkert, A. 2006b, *ApJ*, 636, L81
- Naab, T. & Ostriker, J. P. 2007, *ArXiv Astrophysics e-prints*
- Naab, T. & Trujillo, I. 2006, *MNRAS*, 369, 625
- Navarro, J. F., Frenk, C. S., & White, S. D. M. 1997, *ApJ*, 490, 493
- Nipoti, C., Londrillo, P., & Ciotti, L. 2003, *MNRAS*, 342, 501
- Oppenheimer, B. D. & Davé, R. 2006, *MNRAS*, 373, 1265
- Richstone, D., Ajhar, E. A., Bender, R., Bower, G., Dressler, A., Faber, S. M., Filippenko, A. V., Gebhardt, K., Green, R., Ho, L. C., Kormendy, J., Lauer, T. R., Magorrian, J., & Tremaine, S. 1998, *Nature*, 395, A14+
- Robertson, B., Cox, T. J., Hernquist, L., Franx, M., Hopkins, P. F., Martini, P., & Springel, V. 2006a, *ApJ*, 641, 21
- Robertson, B., Hernquist, L., Cox, T. J., Di Matteo, T., Hopkins, P. F., Martini, P., & Springel, V. 2006b, *ApJ*, 641, 90
- Rothberg, B. & Joseph, R. D. 2006, *AJ*, 132, 976
- Saslaw, W. C., Valtonen, M. J., & Aarseth, S. J. 1974, *ApJ*, 190, 253
- Shakura, N. I. & Syunyaev, R. A. 1973, *A&A*, 24, 337
- Sijacki, D. & Springel, V. 2006, *MNRAS*, 366, 397
- Sijacki, D., Springel, V., di Matteo, T., & Hernquist, L. 2007, *MNRAS*, 380, 877
- Silk, J. & Rees, M. J. 1998, *A&A*, 331, L1
- Sillanpaa, A., Haarala, S., Valtonen, M. J., Sundelius, B., & Byrd, G. G. 1988, *ApJ*, 325, 628
- Springel, V. 2005, *MNRAS*, 364, 1105
- Springel, V., Di Matteo, T., & Hernquist, L. 2005a, *ApJ*, 620, L79
- . 2005b, *MNRAS*, 361, 776
- Springel, V. & Hernquist, L. 2002, *MNRAS*, 333, 649
- . 2003, *MNRAS*, 339, 289
- . 2005, *ApJ*, 622, L9
- Thomas, J., Jesseit, R., Naab, T., Saglia, R. P., Burkert, A., & Bender, R. 2007, *MNRAS*, 381, 1672
- Tran, K.-V. H., van Dokkum, P., Franx, M., Illingworth, G. D., Kelson, D. D., & Schreiber, N. M. F. 2005, *ApJ*, 627, L25
- Tremaine, S., Gebhardt, K., Bender, R., Bower, G., Dressler, A., Faber, S. M., Filippenko, A. V., Green, R., Grillmair, C., Ho, L. C., Kormendy, J., Lauer, T. R., Magorrian, J., Pinkney, J., & Richstone, D. 2002, *ApJ*, 574, 740
- Väisänen, P., Mattila, S., Kniazev, A., Adamo, A., Efstathiou, A., Farrah, D., Johansson, P. H., Ostlin, G., Buckley, D. A. H., Burgh, E. B., Crause, L., Hashimoto, Y., Lira, P., Loaring, N., Nordsieck, K., Romero-Colmenero, E., Ryder, S., Still, M., & Zijlstra, A. 2007, *ArXiv e-prints*, 708
- van Dokkum, P. G. 2005, *AJ*, 130, 2647
- van Dokkum, P. G., Franx, M., Fabricant, D., Kelson, D. D., & Illingworth, G. D. 1999, *ApJ*, 520, L95
- Vitvitska, M., Klypin, A. A., Kravtsov, A. V., Wechsler, R. H., Primack, J. R., & Bullock, J. S. 2002, *ApJ*, 581, 799
- Volonteri, M., Haardt, F., & Madau, P. 2003, *ApJ*, 582, 559
- Wyithe, J. S. B. & Loeb, A. 2003, *ApJ*, 595, 614